A series of two-phase models for grain-fluid flows with dilatancy

F. Bouchut, E. Drach, E.D. Fernández-Nieto, A. Mangeney, G. Narbona-Reina

Supplementary Material

S.A. Two-layer three-velocity model (A1) modified from Bouchut et al. (2016)

The models presented here are derived from our previous work (Bouchut et al. 2016) with slight modifications concerning the rheology and the boundary conditions at the bottom and at the interface between the mixture and the upper fluid layer. Note that the modification of the interface conditions does not affect the one velocity models presented in Section 3 since the associated terms disappear when the total momentum conservation is written. The updated rheology is presented in Section 2.2. We first summarize here the boundary conditions considered for the whole 3-D problem and then we focus on the modified conditions at the bottom and at the interface. We also discuss different alternatives proposed in the literature for these boundary conditions. We then write the energy balance of the modified model. Finally, we develop the derivation of the pressure evolution equation (2.30) presented in section 2.3.2.

S.A.1. *Summary of boundary conditions*

A summary of the boundary conditions considered for the full two-layer model domain is depicted in figure S1. We use the bold uppercase font to denote 3-D vectors and the subscript "tg" for the tangential projection of a vector, that is $\mathbf{W}_{\rm tg} = \mathbf{W} - (\mathbf{W}\cdot\mathbf{N}_X)\mathbf{N}_X$, for any vector $\mathbf{W} = (\mathbf{w}^{\mathbf{x}}, w^z)$ and any normal $\mathbf{N}_X$. See notation in figure S2. Details are given below in sections S.A.2 and S.A.3.

At the bottom we impose a no-penetration condition for the two phases,

$$\mathbf{U}\cdot\mathbf{N}_X^b = \mathbf{V}\cdot\mathbf{N}_X^b = 0, \tag{S.A.1}$$

together with a Coulomb type friction law for the solid and a viscous shear for the fluid,

$$(\sigma_s\mathbf{N}_X^b)_{\rm tg} = -\mu\,\mathrm{sgn}(\mathbf{V})(\sigma_s\mathbf{N}_X^b)\cdot\mathbf{N}_X^b, \tag{S.A.2}$$

$$(\sigma_{f_m}\mathbf{N}_X^b)_{\rm tg} = \frac{5}{2}\frac{\eta_e(1-\varphi)}{h_m}\mathbf{U}_{\rm tg}, \tag{S.A.3}$$

with $\eta_e = \eta_f(1+\frac{5}{2}\varphi)$ the effective fluid viscosity.

At the free surface the kinematic condition is considered for the top fluid velocity

$$\partial_t(b+h_m+h_f) + \mathbf{U}_f\cdot\mathbf{N}_X^{\rm surf} = 0, \tag{S.A.4}$$

and a stress-free condition

$$\sigma_f\mathbf{N}_X^{\rm surf} = 0. \tag{S.A.5}$$

At the mixture/fluid interface we consider that the normal component of the normal stress vanishes and the kinematic conditions for the solid phase

$$(\sigma_s\mathbf{N}_X^i)\cdot\mathbf{N}_X^i = 0, \tag{S.A.6}$$

$$\partial_t(b+h_m) + \mathbf{V}\cdot\mathbf{N}_X^i = 0. \tag{S.A.7}$$

The conservation of the fluid mass is given by the following relation where we also introduce the fluid transfer rate $\mathcal{V}_f$,

$$\mathcal{V}_f \equiv \partial_t(b+h_m) + \mathbf{U}_f\cdot\mathbf{N}_X^i = (1-\varphi)(\partial_t(b+h_m) + \mathbf{U}\cdot\mathbf{N}_X^i). \tag{S.A.8}$$

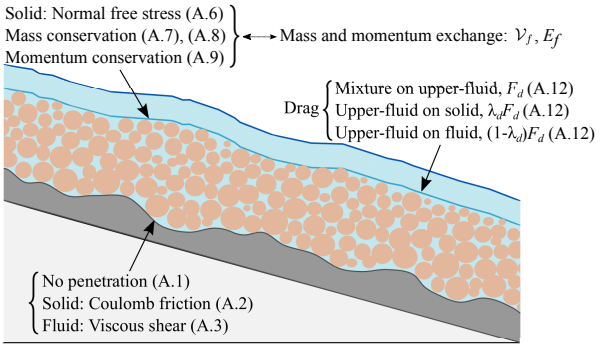

Figure S1: Summary of the boundary conditions at the bottom and at the interface between the mixture and upper fluid layers for the full two-layer model with three velocities (A1) and references to the corresponding equations. Additionally, a kinematic and stress-free condition for the upper-fluid is considered at the free surface, given in (S.A.4), (S.A.5).

We impose the total momentum conservation

$$\rho_f \mathcal{V}_f(\mathbf{U}_f - \mathbf{U}) + (\sigma_s + \sigma_{f_m})\mathbf{N}_X^i = \sigma_f \mathbf{N}_X^i, \tag{S.A.9}$$

where the stress tensors are $\sigma_j = -p_j \mathrm{Id} + \sigma_j'$, for $j = s, f_m, f$. In order to determine the tangent component of the stress tensor at the interface for each constituent, two more conditions are needed. First we denote by E_f the tangential projection of the flux of fluid momentum through the interface appearing in the first term of (S.A.9),

$$E_f = \rho_f \mathcal{V}_f(\mathbf{U}_f - \mathbf{U})_{\mathrm{tg}}. \tag{S.A.10}$$

Then, we introduce a drag between the fluid in the upper layer and the mixture

$$F_d = k_f(\mathbf{U}_f - \mathbf{V}_m)_{\mathrm{tg}}, \tag{S.A.11}$$

where the 3-D mixture velocity is $\mathbf{V}_m = \frac{1}{\rho}(\rho_s \varphi \mathbf{V} + \rho_f(1-\varphi)\mathbf{U})$. The distribution of the fluid transfer (E_f) and of the drag (F_d) components is made through two distribution coefficients λ_f and λ_d respectively in such a way that

$$\begin{aligned} (\sigma_s \mathbf{N}_X^i)_{\mathrm{tg}} &= \lambda_d F_d, \\ (\sigma_{f_m} \mathbf{N}_X^i)_{\mathrm{tg}} &= (1-\lambda_d)F_d - \lambda_f E_f, \\ (\sigma_f \mathbf{N}_X^i)_{\mathrm{tg}} &= F_d + (1-\lambda_f)E_f. \end{aligned} \tag{S.A.12}$$

They are defined as

$$\begin{aligned} &\lambda_d = \tfrac{\varphi \rho_s}{\rho}, \\ &\lambda_f = \tfrac{1}{2} - \tfrac{1}{2}\,\mathrm{sgn}(\mathcal{V}_f)\delta_f, \quad \delta_f = \begin{cases} 0 & \text{centered distribution,} \\ 1 & \text{upwind distribution.} \end{cases} \end{aligned} \tag{S.A.13}$$

To summarize, if $\delta_f = 0$ the fluid velocity at the interface is $(\mathbf{U} + \mathbf{U}_f)/2$, while if $\delta_f = 1$, it is given in terms of the sign of $\mathcal{V}_f$. Thus, if the fluid is expelled from the mixture (contraction), $\mathcal{V}_f > 0, \lambda_f = 0$ so that the velocity is $\mathbf{U}$. On the contrary, if the fluid is sucked into the mixture (dilation), $\mathcal{V}_f < 0, \lambda_f = 1$ and the velocity is $\mathbf{U}_f$.

S.A.2. *Fluid viscous shear at the bottom*

In the model proposed in Bouchut et al. (2016), viscosity effects are neglected in the total stress tensor but are present in the form of a friction boundary condition specified in the xz

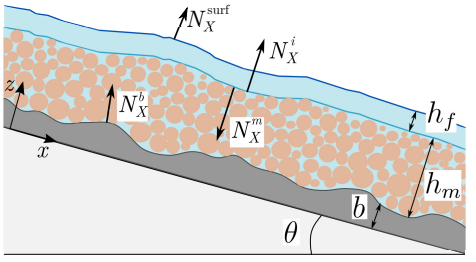

Figure S2: Notations for two-layer models (groups A and B).

component of the stress tensors at the base of the flow. On the contrary the Iverson-George model (Iverson & George 2014) considered the viscous stress at the bottom. The basal friction condition for the fluid phase used in Bouchut et al. (2016) was established as

$$(\sigma_{f_m}\mathbf{N}_X^b)_{\text{tg}} = k_b\mathbf{U}_{\text{tg}} + O(\epsilon^3) \quad \text{at the bottom.} \tag{S.A.14}$$

If we consider $\sigma_{f_m} = -p_{f_m}\text{Id} + \sigma'_{f_m}$ with $\sigma'_{f_m} = 2(1-\varphi)\eta_e D(\mathbf{U})$, for η_e the effective fluid viscosity and $D(\mathbf{U})$ the fluid strain rate tensor, we obtain that $(\sigma_{f_m}\mathbf{N}_X^b)_{\text{tg}} = \sigma_{f_m}^{xz} = (1-\varphi)\eta_e\partial_z\mathbf{u}^{\mathbf{x}} + O(\epsilon^3)$ when $\eta_e = O(\epsilon^2)$. By approximating $\partial_z\mathbf{u}^{\mathbf{x}}{}_{|b} \sim c_b\mathbf{u}^{\mathbf{x}}/h_m$, for some constant c_b we write

$$(1-\varphi)\eta_e c_b\frac{\mathbf{u}^{\mathbf{x}}}{h_m} = k_b\mathbf{u}^{\mathbf{x}} + O(\epsilon^3) \quad \text{at the bottom,}$$

leading to $k_b = c_b\frac{\eta_e(1-\varphi)}{h_m}$. This expression is similar to the one considered by Iverson and George in Iverson & George (2014) given by τ_f in equation (3.18*a*) for $c_b = 2$ and $h_m \sim h$. For consistency with our approximation of the shear rate, we consider in this work $c_b = \frac{5}{2}$, then following (S.A.14) the coefficient k_b reads

$$k_b = \frac{5}{2}\frac{\eta_e(1-\varphi)}{h_m}, \quad \text{with} \quad \eta_e = \eta_f\left(1+\frac{5}{2}\varphi\right), \tag{S.A.15}$$

that gives (S.A.3). We discuss other alternatives in section S.A.4.1.
Note that the effect of fluid viscosity is also present in the viscous number J. As the empirical relation defining J is usually built up from lab-scale experiments, it is hard to discriminate between the fluid viscous term and the solid-fluid drag. As a result as to whether this fluid friction has to be added in the equations involving a rheology with viscous-inertial numbers fitted on lab-experiments is still an open issue [E. Guazzelli, personal communication].

S.A.3. *Drag at the upper-fluid/mixture interface*

At the interface between the upper fluid layer and the mixture, exchange of fluid mass occurs and corresponds to $\mathcal{V}_f$. When $\mathcal{V}_f > 0$, the fluid is expelled from the mixture towards the fluid-only region. In figure S2 we specify the notation of the normal vectors in the domain. We remind that the 3-D velocities are $\mathbf{V} = (\mathbf{v}^{\mathbf{x}}, v^z), \mathbf{U} = (\mathbf{u}^{\mathbf{x}}, u^z), \mathbf{U}_f = (\mathbf{u}_f^{\mathbf{x}}, u_f^z)$.
In Bouchut et al. (2016) the drag between the two layers reduced to the drag force between the fluid phases in the upper and mixture layers and it was written as $k_f(\mathbf{U}_f - \mathbf{U})$ with $k_f \geq 0$ a friction coefficient. It seems however more suitable to consider instead a drag between the upper fluid and the mixture as a whole. We thus specify

$$F_d = k_f(\mathbf{U}_f - \mathbf{V}_m)_{\text{tg}}, \tag{S.A.16}$$

where $(\mathbf{V}_m)_{\text{tg}}$ is the value of the tangent component of the 3-D velocity of the mixture at the interface. Note that we must decide which part of this drag stress is experienced by each of the phases in the mixture. Let us denote F_{d_s} and F_{d_f}, the drag exerted by the upper-fluid on the solid and fluid phase in the mixture, respectively. Then $F_d = F_{d_f} + F_{d_s}$ is split into these two components:

$$F_{d_s} = \lambda_d F_d \quad \text{and} \quad F_{d_f} = (1-\lambda_d)F_d, \tag{S.A.17}$$

for some non-negative coefficient λ_d. In order to obtain a dissipative contribution to the energy of the system (see (S.A.26)), this coefficient must be taken such that $\mathbf{V}_m = \lambda_d \mathbf{V} + (1-\lambda_d)\mathbf{U}$. Then we propose to take the distribution parameter as the relative solid density,

$$\lambda_d = \frac{\varphi \rho_s}{\rho}. \tag{S.A.18}$$

In this case, the contribution to the energy of the depth-averaged model is given by the term, $-k_f|\mathbf{u}_f - \mathbf{v}_m|^2$.

As in Bouchut et al. (2016), the conservation of the total momentum is given in (S.A.9) and E_f in (S.A.10) is the tangential flux of fluid momentum through the interface. If we write the tangent component of (S.A.9) it reads

$$(\sigma_f \mathbf{N}_X^i)_{\text{tg}} - (\sigma_s \mathbf{N}_X^i)_{\text{tg}} - (\sigma_{f_m} \mathbf{N}_X^i)_{\text{tg}} = E_f.$$

Taking into account $\mathbf{N}_X^m = -\mathbf{N}_X^i$ (see figure S2) it becomes

$$(\sigma_f \mathbf{N}_X^i)_{\text{tg}} + (\sigma_s \mathbf{N}_X^m)_{\text{tg}} + (\sigma_{f_m} \mathbf{N}_X^m)_{\text{tg}} = E_f.$$

We see that there is a contribution to the shear stress due to the fluid flux at the interface related to E_f. How E_f should be distributed between the different fluid stresses $(\sigma_f \mathbf{N}_X^i)_{\text{tg}}, (\sigma_{f_m} \mathbf{N}_X^m)_{\text{tg}}$ is an open question and should be further studied. See discussion in section S.A.4.2. In general we consider a non-negative distribution coefficient λ_f in such a way that $(1-\lambda_f)E_f$ is the part of the fluid flux applied by the upper-fluid on the whole mixture. Thus, we assume that the tangential stress applied by the upper-fluid to the mixture at the interface entails the drag stress and part of the fluid mass exchange given by $(1-\lambda_f)E_f$:

$$\sigma_{\text{tg}}^{\text{on mix}} = (\sigma_f \mathbf{N}_X^i)_{\text{tg}} = (\sigma_f \mathbf{N}_X^i) - ((\sigma_f \mathbf{N}_X^i)\cdot \mathbf{N}_X^i)\mathbf{N}_X^i = F_d + (1-\lambda_f)E_f. \tag{S.A.19a}$$

On the other hand, the stress exerted to the upper fluid layer by the mixture comes from the grain and fluid phases. The contribution of the fluid phase is given by the addition of the drag F_{d_f} and the corresponding fluid mass exchange to ensure (S.A.9),

$$\sigma_{\text{tg}}^{\text{on up fluid,f}} = (\sigma_{f_m} \mathbf{N}_X^m)_{\text{tg}} = (\sigma_{f_m} \mathbf{N}_X^m) - ((\sigma_{f_m} \mathbf{N}_X^m)\cdot \mathbf{N}_X^m)\mathbf{N}_X^m = -(1-\lambda_d)F_d + \lambda_f E_f. \tag{S.A.19b}$$

The contribution of the solid phase at the interface in the tangent direction (considering $\mathbf{N}_X^m = -\mathbf{N}_X^i$) is instead just given by the corresponding drag F_{d_s},

$$\sigma_{\text{tg}}^{\text{on up fluid,s}} = (\sigma_s \mathbf{N}_X^m)_{\text{tg}} = (\sigma_s \mathbf{N}_X^m) - ((\sigma_{s_m} \mathbf{N}_X^m)\cdot \mathbf{N}_X^m)\mathbf{N}_X^m = -\lambda_d F_d. \tag{S.A.19c}$$

We notice that adding (S.A.19*a*), (S.A.19*b*) and (S.A.19*c*) we recover (S.A.9), taking into account that $\mathbf{N}_X^m = -\mathbf{N}_X^i$. Therefore only two of the three equations (S.A.19*a*), (S.A.19*c*), (S.A.19*b*) are necessary since the last one can be obtained from the tangent part of (S.A.9).

We will take here two possible distributions, called centered and upwind with respect to the sign of the fluid mass flux $\rho_f \mathcal{V}_f$ and defined by the distribution coefficient λ_f, that may depend on dilation/contraction, as

$$\lambda_f = \frac{1}{2} - \frac{1}{2}\,\text{sgn}(\mathcal{V}_f)\delta_f, \quad \delta_f = \begin{cases} 0 & \text{centered distribution,} \\ 1 & \text{upwind distribution.} \end{cases} \tag{S.A.20}$$

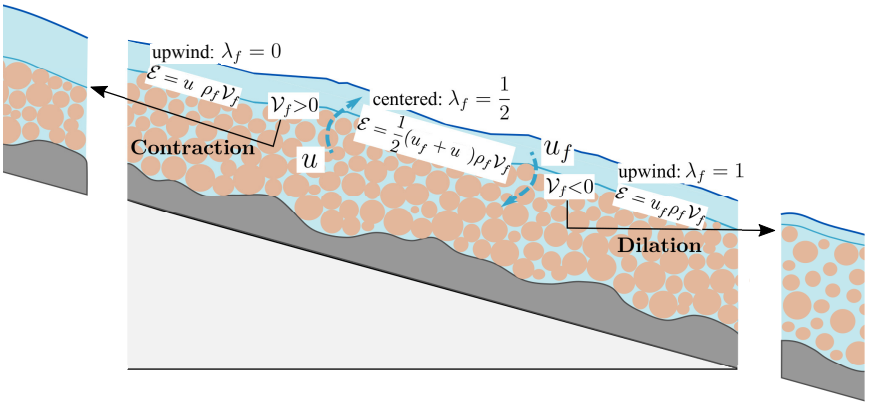

Figure S3: Tangent fluid momentum distribution at the interface. When $\mathcal{V}_f > 0$ the fluid is transferred from the mixture to the upper-fluid layer, thus the interface goes down (picture on the left). When $\mathcal{V}_f < 0$ the fluid is transferred from the upper-fluid layer to the mixture, and the interface goes up (picture on the right). $\mathcal{E} = ((1-\lambda_f)\mathbf{u} + \lambda_f \mathbf{u}_f)\rho_f \mathcal{V}_f$ represents the term appearing in the momentum equation for each phase (see equations (2.18*b*) and (2.18*c*))

In figure S3 we present a schematic view of the implications of this definition.

For the centered choice, $\lambda_f = 1/2$, the term E_f is equally distributed between the stresses exerted on both layers by one layer to the other. In the upwind approximation $\lambda_f = 0$ when $\mathcal{V}_f > 0$, *i.e.* in case of contraction when the fluid is transferred from the mixture to the upper fluid layer (picture on the left side in figure S3). The term E_f thus only contributes to the stress applied by the upper-fluid to the mixture at the interface and just appears in $\sigma_{\text{tg}}^{\text{on mix}} = (\sigma_f \mathbf{N}_X^i)_{\text{tg}}$. On the contrary, when the granular mass dilates $\mathcal{V}_f < 0$ which means that the fluid is sucked by the mixture layer from the upper fluid layer, $\lambda_f = 1$ and thus the term E_f only contributes to the stress applied by the fluid mixture to the upper-fluid at the interface (picture on the right side in figure S3). As a result, it just appears in $\sigma_{\text{tg}}^{\text{on up fluid,f}} = (\sigma_{f_m} \mathbf{N}_X^m)_{\text{tg}}$. The corresponding term appearing in the energy equation of the depth-averaged model is calculated as

$$\left(\lambda_f - \frac{1}{2}\right) \rho_f \mathcal{V}_f |\mathbf{u}_f - \mathbf{u}|^2 = -\frac{1}{2} \delta_f \rho_f |\mathcal{V}_f|\, |\mathbf{u}_f - \mathbf{u}|^2. \tag{S.A.21}$$

This choice thus ensures a dissipative contribution to the energy balance. In particular for the centered distribution no contribution is made to the energy since $\delta_f = 0$. Although to our knowledge, there is no measurements or physical reasons to choose one of these approximations (or even others), these choices lead to a dissipative or to no contribution in the energy balance of the derived model (see equation (S.A.26)).

The resulting term describing the fluid mass exchange in the depth-averaged model is given by $\mathcal{E} = ((1-\lambda_f)\mathbf{u} + \lambda_f \mathbf{u}_f)\rho_f \mathcal{V}_f$, appearing in the momentum equations of the fluid in the mixture (2.18*b*) and in the upper layer (2.18*c*)). We see that the distribution coefficient λ_f finally describes the velocity at the interface, given as a convex combination of the fluid in the upper-fluid layer and the fluid in the mixture, $(1-\lambda_f)\mathbf{u} + \lambda_f \mathbf{u}_f$, see figure S3. Under this interpretation, we think that the better choice is to consider the averaged velocity, that is, $\frac{1}{2}(\mathbf{u}_f + \mathbf{u})$, given by the centered approximation $\lambda_f = \frac{1}{2}$, as in our previous work (Bouchut et al. 2016).

It should be pointed out here that the issue of prescribing physically meaningful conditions at this interface comes from the depth-averaged processes that requires to link discontinuous depth-averaged quantities at an interface (see figure S4). However, in a real 3-D situation

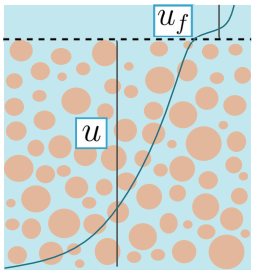

Figure S4: Illustration of the real velocity profile in the fluid phase in blue and depth-averaged fluid velocities $\mathbf{u}$ and $\mathbf{u}_f$ considered in the two-layer depth-averaged models.

the fluid is a continuous media and there is no discontinuity of the velocity as illustrated in figure S4, that shows an example of a real velocity profile and of the averaged velocity of the fluid in the mixture $\mathbf{u}$ and in the upper-fluid layer $\mathbf{u}_f$. A similar problem occurs when trying to describe erosion/deposition processes (static/flowing interface) in depth-averaged models (see *i.e.* (Bouchut et al. 2008)). For this reason, one-layer models that imply adding these interface conditions (they thus do not appear anymore), eliminate these approximations.

S.A.4. *Alternative descriptions proposed in the literature*

We present here similar conditions considered in the literature, other than in the Iverson and George and Meng and Wang models that have been thoroughly analyzed in this paper (see also section S.B.2.2 for a detailed comparison of the boundary conditions with the Meng-Wang model). We analyze three descriptions that are relevant in the model, namely, the viscous shear, the drag and exchange conditions at the mixture/upper-fluid interface, and the inter-phase drag between solid and fluid phases in the mixture. In particular we study the works in Luca et al. (2012); Meng et al. (2022); Sun et al. (2023); Baumgarten & Kamrin (2019).

For the reader convenience we briefly remind the main characteristics of the models proposed in those papers. In Luca et al. (2012) a 2-D depth-averaged two-layer model for over-saturated debris flows taking into account the bottom curvature is presented. The model accounts for two velocities in the mixture and one independent velocity for the upper-fluid layer, as in our full model (A1). Nevertheless dilatancy effects and rheology are not considered. In Meng et al. (2022) a 1-D depth-averaged model for debris flows is proposed dealing with transitions from pure fluid/solid configurations to under-saturated or over-saturated mixture. This model also does not account for dilatancy, rheology nor mass exchange. In Sun et al. (2023) a 1-D depth-averaged two-phase model is presented for submarine avalanches. This model takes into account the dilatancy and mass exchange, it considers one velocity for the mixture and an independent velocity for the upper-fluid layer, as in our model (A2). Finally, in Baumgarten & Kamrin (2019) a 3-D two-phase model for fluid saturated sediment is presented from the Jackson's equations. To close the system a thermodynamic analysis of a two-phase mixture, for elastic-plastic granular solid in a viscous fluid is performed. The model accounts for mixture rheology and dilatancy effects. This model is especially relevant for the closures of the 3-D starting model (Jackson's model), namely the viscous tensor and the inter-phase friction. Moreover, as said in section 2.3.2, the evolution equation for the solid pressure presented here is inspired by this work.

S.A.4.1. *Fluid viscous stress and basal fluid shear stress at the bottom*

In section S.A.2 we introduced a way to take into account the fluid viscosity in our depth-averaged model through the approximation of the viscous fluid stress at the bottom in the

corresponding boundary condition, as proposed in Iverson & George (2014). The total stress is defined as $\sigma_{f_m} = -p_{f_m}\mathrm{Id} + \sigma'_{f_m}$ with $\sigma'_{f_m} = 2(1-\varphi)\eta_e D(\mathbf{U})$, for η_e the effective fluid viscosity. The boundary condition then reading

$$(\sigma_{f_m}\mathbf{N}_X^b)_{\mathrm{tg}} = \frac{5}{2}\frac{(1-\varphi)\eta_e}{h_m}\mathbf{U}_{\mathrm{tg}} \quad \text{at the bottom.}$$

In Luca et al. (2012) the fluid viscosity is neglected and a quadratic friction law is considered at the bottom, namely $(\sigma_{f_m}\mathbf{N}_X^b)_{\mathrm{tg}} = c_b(1-\varphi)\mathbf{U}\|\mathbf{U}\|$ with c_b a constant coefficient. In contrast, in models proposed in Meng et al. (2022); Sun et al. (2023) the downslope component of the fluid viscous stress is kept in the depth-averaged model, providing the term $\partial_x(h_m 2\eta_f(1-\varphi)\partial_x\mathbf{u})$. In that case, the viscous shear at the bottom is not considered. In Sun et al. (2023) no drag for the fluid at the bottom is considered, so this term is just neglected. In Meng et al. (2022) the viscous shear at the bottom is replaced with a Chézy drag, $(\sigma_{fm}\mathbf{N}_X^b)_{\mathrm{tg}} = C_{\mathrm{Ch}}\rho_f\mathbf{U}\|\mathbf{U}\|$ with C_{Ch} a Chézy drag coefficient. As explained in section 4.3.2 this choice, also considered in Meng & Wang (2018), seems to be inconsistent when viscosity is taking into account in the model. The use of the effective viscosity in the stress tensor is also considered in Baumgarten & Kamrin (2019) for their 3-D model.

S.A.4.2. *Drag and mass exchange at the interface*

These interface conditions have been described and discussed in section S.A.3 (equations (S.A.10)-(S.A.13)). We present here alternative conditions considered in the literature for similar models, namely in Luca et al. (2012); Meng et al. (2022); Sun et al. (2023).

Let us begin with the over-saturated mixture model proposed in Luca et al. (2012). At the interface, the conservation of the total momentum (S.A.9) is considered and in particular the stress of the upper layer is distributed in terms of the solid volume fraction, such that†

$$\sigma_{f_m}\mathbf{N}_X^i = (1-\varphi)(\sigma_f\mathbf{N}_X^i) - \rho_f\mathcal{V}_f(\mathbf{U}_f - \mathbf{U}), \qquad \sigma_s\mathbf{N}_X^i = \varphi(\sigma_f\mathbf{N}_X^i). \tag{S.A.22}$$

Notice that, unlike in our model (equations (S.A.12)), the distribution is performed for the total stress and not only for the tangential component. This has an important impact on the calculated pressures, as detailed below. Additionally, the following friction law at the interface is proposed (see equation (103) in that paper)

$$(\sigma_f\mathbf{N}_X^i)_{\mathrm{tg}} = C|(\mathbf{U}_f - \mathbf{V}^{\mathrm{Luca}})_{\mathrm{tg}}|(\mathbf{U}_f - \mathbf{V}^{\mathrm{Luca}})_{\mathrm{tg}} = F_d^{\mathrm{Luca}}$$

for a constant coefficient C and with $\mathbf{V}^{\mathrm{Luca}} = \varphi\mathbf{V} + (1-\varphi)\mathbf{U}$, that also differs from our mixture velocity $\mathbf{V}_m = \frac{1}{\rho}(\rho_s\varphi\mathbf{V} + \rho_f(1-\varphi)\mathbf{U})$. If we write the tangential components of these expressions we find that

$$\begin{aligned}(\sigma_s\mathbf{N}_X^i)_{\mathrm{tg}} &= \varphi F_d^{\mathrm{Luca}},\\ (\sigma_{f_m}\mathbf{N}_X^i)_{\mathrm{tg}} &= (1-\varphi)F_d^{\mathrm{Luca}} - E_f,\\ (\sigma_f\mathbf{N}_X^i)_{\mathrm{tg}} &= F_d^{\mathrm{Luca}}.\end{aligned} \tag{S.A.23}$$

When compared with our conditions (S.A.12), we find that $\lambda_d^{\mathrm{Luca}} = \varphi$ and $\lambda_f^{\mathrm{Luca}} = 1$. Their definition of the distribution parameter λ_d, representing the contribution of the drag to the solid phase, follows the same idea than in our equations (S.A.17)-(S.A.18). In our case $\lambda_d = \varphi\rho_s/\rho$ which is the coefficient related to the solid velocity $\mathbf{V}$ in the expression of our mixture velocity $\mathbf{V}_m$. Analogously, $\lambda_d^{\mathrm{Luca}} = \varphi$ corresponds to the coefficient before $\mathbf{V}$ in their

† With the notation in Luca et al. (2012), $\mathcal{M}_{int} = \rho_f\mathcal{V}_f$, $v_2 = \mathbf{u}_f$, $\upsilon = \varphi$, so $E_f = -\mathcal{M}_{int}(\mathbf{u} - v_2)_{\mathrm{tg}}$. See their equations (22)-(24) and (37)-(38).

mixture velocity $\mathbf{V}^{\text{Luca}}$. This choice ensures a dissipative contribution to the energy in their model with the term $-C|\mathbf{u}_f - \mathbf{v}^{\text{Luca}}|^3$, with $\mathbf{v}^{\text{Luca}} = \varphi\mathbf{v} + (1-\varphi)\mathbf{u}$.

On the contrary, the choice $\lambda_f^{\text{Luca}} = 1$ does not ensure a dissipative contribution to the energy related to the fluid exchange. Following (S.A.21) the corresponding term appearing in the energy equation would be

$$\frac{1}{2}\rho_f \mathcal{V}_f |\mathbf{u}_f - \mathbf{u}|^2.$$

This term does not have a fixed sign since it depends on the sign of $\mathcal{V}_f$. Furthermore, in view of (S.A.23), the value λ_f^{Luca} does not distribute the fluid mass between the two fluid tangent tensors since it is only present in the mixture fluid tensor σ_{f_m}, thus preventing a description of the case where the fluid goes out from the mixture. Following (S.A.20) it seems that the only considered case is the dilation regime where the fluid is sucked by the mixture layer. The final model presented in Luca et al. (2012) does not account for fluid exchange since they consider $\mathcal{V}_f = 0$. However, in section 4.2 of their paper, the authors discuss the need of an additional closure for this term since they do not consider dilatancy. In our model this closure is indeed given by the dilatancy law that allows to obtain the explicit expression of the fluid transfer rate $\mathcal{V}_f$.

Their conditions (S.A.22) have also an important consequence on the pressure of each phase. The layer above contributes with the quantity $(1-\varphi)(\sigma_f \mathbf{N}_X^i)\mathbf{N}_X^i$ to the normal stress of the fluid phase in the mixture, but also with $\varphi(\sigma_f \mathbf{N}_X^i)\mathbf{N}_X^i$ to the normal stress of the solid phase. Namely, the pressures at the interface are given by (see equation 79 in Luca et al. (2012)), $p_{s\,|b+h_m} = \frac{\rho_f}{\rho_s}\varphi p_{f\,|b+h_m}$, $p_{f_m\,|b+h_m} = (1-\varphi)p_{f\,|b+h_m}$. These values affect the basal solid pressure and thus the Coulomb frictional stress. In Luca et al. (2012), if we neglect the curvature effect, the solid pressure at the bottom reads†

$$\begin{aligned} p_{s\,|b}^{\text{Luca}} &= \varphi g\cos\theta\rho_s(h_m + \frac{\rho_f}{\rho_s}h_f) = \varphi g\cos\theta(\rho_s h_m + \rho_f h_f) \\ &= \varphi g\cos\theta(\rho_s - \rho_f)h_m + \varphi g\cos\theta\rho_f(h_m + h_f) \end{aligned}$$

This expression differs from ours since the authors add to the solid pressure the pressure applied by the fluid layer above while we consider that the separation of the fluid and solid stress tensors induces that the pressure from the upper fluid layer is only supported by the fluid phase.

On the contrary, in our model, we assume that the solid normal stress does not receive any contribution from the liquid layer above (see equations (S.A.6)). The weight of the upper fluid layer is thus supported by the fluid in the mixture, by assuming that the normal stress is continuous at the interface. The solid phase pressure is of course affected by the pressure of the fluid, but it appears in the buoyancy force given by the term $-\varphi\rho_f g\cos\theta h_m$, that is involved in the resulting solid pressure at the bottom

$$p_{s\,|b} = \varphi(\rho_s - \rho_f)g\cos\theta h_m - (p_{f_m}^e)_{|b}$$

(see remark 2 below).

Let us now comment on the depth-averaged model for submarine avalanches presented in Sun et al. (2023) where dilatancy and mass exchange are taken into account. Three different velocities are considered but the sediment layer is treated as a mixture with velocity $\mathbf{V}_m$. The total momentum conservation is considered as in (S.A.9) and the friction at the interface

† see equation 82 in that paper or the one dimensional model stated in section 5 of Luca et al. (2012)

reads

$$\begin{aligned}\rho_f \mathcal{V}_f(\mathbf{U}_f - \mathbf{U}) &= (\sigma_f - (\sigma_s + \sigma_{f_m}))\mathbf{N}_X^i,\\ (\sigma_f \mathbf{N}_X^i)_{\text{tg}} &= (\sigma_{f_m}\mathbf{N}_X^i)_{\text{tg}} = C(\mathbf{U}_f - \mathbf{V}_m) = F_d^{\text{Sun}}.\end{aligned} \tag{S.A.24}$$

where C is a coefficient depending on the permeability†. We combine these conditions to write the tangential components of these expressions,

$$\begin{aligned}(\sigma_s \mathbf{N}_X^i)_{\text{tg}} &= -E_f,\\ (\sigma_{f_m}\mathbf{N}_X^i)_{\text{tg}} &= F_d^{\text{Sun}},\\ (\sigma_f \mathbf{N}_X^i)_{\text{tg}} &= F_d^{\text{Sun}}.\end{aligned} \tag{S.A.25}$$

Notice that since the sediment layer is considered as a whole, the total stress $\sigma_s + \sigma_{f_m}$ must be considered as the stress in this mixture layer. Hence an equivalence with our proposal in (S.A.12), gives $\lambda_d^{\text{Sun}} = 0$ and $\lambda_f^{\text{Sun}} = 1$. The first one tells that the solid phase does not experience any friction with the upper-fluid layer. The second one would be equivalent to the proposal in Luca et al. (2012), written in (S.A.23), carrying the same non-dissipative term in the energy balance. Although it is not clearly exposed in Sun et al. (2023), the authors consider the continuity of the fluid pressure at the interface, so the solid pressure at the bottom is correctly calculated (see equations B18-B19 in Sun et al. (2023)). Nevertheless it is wrongly written in equation (46) of Sun et al. (2023) where they present the final model.

Finally, in the debris flow model proposed in Meng et al. (2022), these effects are neglected, even for the over-saturated case, and no mass exchange nor friction are considered at the interface.

Remark 2 (Meaning of the solid stress). *In several works in the literature dealing with two-phase flows, as for example in (Baumgarten & Kamrin 2019; Meng et al. 2022; Sun et al. 2023), the total solid stress tensor is defined as*‡

$$\sigma_s^T = \sigma_s - \varphi p_{f_m}\,\text{Id},$$

where σ_s is called the effective solid stress. The second term holds the effect of the pore pressure exerted on the granular phase and it gives the buoyancy term in the Jackson equations. To quote Baumgarten & Kamrin (2019),

> The effective granular stress σ_s is the portion of the solid phase stress resulting from granular contact forces and from microscopic viscous stresses on grains from the fluid medium; it excludes the pressurization of the grains due to the pressure of the pore fluid.

Thus, when viscous effects are neglected, the stress tensor σ_s only contains the interaction effects between grains themselves without any influence of the fluid pressure. Therefore it is natural to assume that the solid phase pressure does not receive any contribution of the fluid layer above since it is taken by the pore pressure and the effect of the pore fluid is already present in the buoyancy force.

S.A.4.3. *Inter-phase friction*

The inter-phase drag force in the mixture is already present in the 3-D Jackson system. Besides the pure friction effect between phases −that for example disappear when only one velocity is considered for the mixture, as in Iverson & George (2014); Sun et al. (2023) or for our models (A2), (B2), (C2)− this term is directly related to the dilatancy through the pore fluid pressure $p_{f_m}^e$, therefore appearing in the model if dilatancy is considered (see section

† This term is never explicitly stated in the paper, since it is neglected arguing that this friction effect is not important for the performed applications

‡ In Meng et al. (2022) it is said that this notation was originally introduced in de Boer & Ehlers (1990)

2.4).
In our 3-D starting model this term, taken from Pailha & Pouliquen (2009), is given by

$$\beta(\mathbf{V}-\mathbf{U}), \quad \text{with} \quad \beta = (1-\varphi)^2\frac{\eta_f}{k} \quad \text{and} \quad k = \frac{(1-\varphi)^3 d^2}{150\varphi^2},$$

k being the permeability, leading to the coefficient (see equation (2.21))

$$\beta = \frac{150\varphi^2}{(1-\varphi)d^2}\eta_f.$$

Notice that in the depth-averaged model presented in section 2.3, this term is kept with the downslope depth-averaged velocities, $\beta(\mathbf{v}-\mathbf{u})$, and the vertical component appears in the excess pore pressure. We present here different proposed values of the coefficient β (Luca et al. 2012; Meng et al. 2022; Sun et al. 2023; Baumgarten & Kamrin 2019).

In the model proposed in Luca et al. (2012), β is assumed to be constant. We have seen however here how much its value that depend on the grain diameter may change the flow behavior. For the submarine avalanches model in Sun et al. (2023), the expression of Pailha & Pouliquen (2009) is adopted for the 3-D system, as in our case. Nevertheless, since only one velocity is considered in the mixture, the force $\beta(\mathbf{v}-\mathbf{u})$ does not appear in the final depth-averaged model.

In their debris flows model (Meng et al. 2022) used

$$\beta^{\text{Meng}} = (1-\varphi)^2\frac{\eta_f}{k^{\text{Meng}}} \quad \text{and} \quad k^{\text{Meng}} = \frac{(1-\varphi)^3 d^2}{180\varphi^2}.$$

The only difference with our model is the coefficient 180 instead of 150. In fact, this value can be deduced from the 3-D model proposed in Baumgarten & Kamrin (2019). In this paper, the inter-phase friction coefficient reads (see equation 2.17 in Baumgarten & Kamrin (2019))

$$\beta(\hat{F}) = \frac{18\varphi(1-\varphi)}{d^2}\eta_f\hat{F},$$

where $\hat{F}$ is a function depending on the volume fraction and the Reynolds number. This function is defined as follows for $0.1 < \varphi < 0.6$ and for low Reynolds number,

$$\hat{F} = \frac{10\varphi}{(1-\varphi)^2} + (1-\varphi)^2\left(1+\frac{3}{2}\sqrt{\varphi}\right).$$

Equivalently, we can also write the corresponding permeability for the model in Baumgarten & Kamrin (2019) as

$$k(\hat{F}) = \frac{(1-\varphi)d^2}{18\varphi\hat{F}}, \quad \text{for} \quad \beta(\hat{F}) = (1-\varphi)^2\frac{\eta_f}{k(\hat{F})}$$

The second term of $\hat{F}$ that we denote $\hat{F}_2 = (1-\varphi)^2\left(1+\frac{3}{2}\sqrt{\varphi}\right)$ is small compared to the first one $\hat{F}_1 = \frac{10\varphi}{(1-\varphi)^2}$ for high values of φ (see inset figure in figure S5a), hence a good approximation would be

$$\hat{F} \simeq \hat{F}_1 = \frac{10\varphi}{(1-\varphi)^2}, \qquad \text{that leads to} \quad \beta(\hat{F}) \simeq \beta(\hat{F}_1) = \frac{180\varphi^2}{(1-\varphi)d^2}\eta_f.$$

This coefficient thus coincides with the one proposed in Meng et al. (2022), that is, $\beta^{\text{Meng}} = \beta(\hat{F}_1)$ and $k^{\text{Meng}} = k(\hat{F}_1)$. In figure S5(left) we show the values of these different coefficients that are pretty close. As observed in our numerical simulations in section 5.3.1 the models

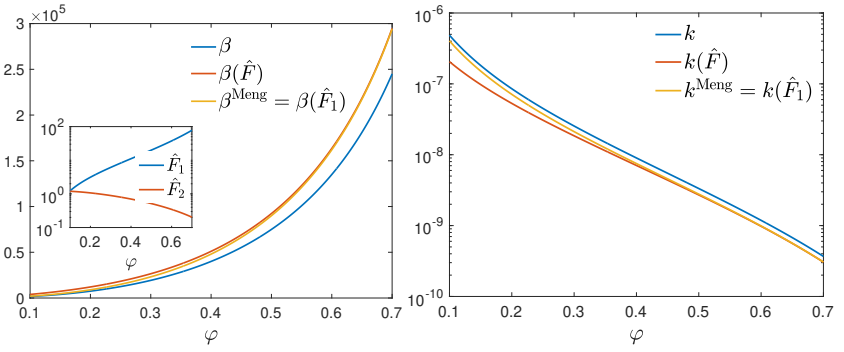

Figure S5: Illustration of the inter-phase drag friction coefficients considered here and in Baumgarten & Kamrin (2019); Meng et al. (2022), as a function of the solid volume fraction φ and for $d = 10^{-3}$m and $\eta_f = 10^{-3}$ Pa s. Left: Friction coefficients β, $\beta(\hat{F})$ and β^{Meng}. Inset figure: Functions $\hat{F}_1 = \frac{10\varphi}{(1-\varphi)^2}$ and $\hat{F}_2 = (1-\varphi)^2\left(1+\frac{3}{2}\sqrt{\varphi}\right)$. Right: Permeability for the three models.

are very sensitive to the permeability. The values of the permeability in the models discussed here do not differ too much except for small volume fraction as shown in figure S5(right). In contrast, the values proposed by Iverson and George in Iverson & George (2014) are at least two orders of magnitude bigger (figure S14).

More complex expression for β can be found in the recent papers (Montellà et al. 2021, 2023) where a 3-D model for immersed granular avalanches with dilatancy is proposed. A quadratic friction is considered here, namely

$$\beta^{\text{Mont.}} = (1-\varphi)^2\frac{\eta_f}{k^{\text{Mont.}}} \quad \text{with} \quad k^{\text{Mont.}} = \frac{(1-\varphi)^2 d^2}{\alpha_E\,\varphi^2} + \frac{(1-\varphi)^3 d\eta_f}{\beta_E\,\rho_f|\mathbf{V}-\mathbf{U}|},$$

where the permeability is originally proposed in Engelund (1953). The calibration parameters α_E varies from 780 to 1500 or more and β_E from 1.8 to 3.6 or more. In Montellà et al. (2023) the authors show the influence of the permeability in their model through numerical results. Notice that if we neglect the second term in the permeability $k^{\text{Mont.}}$ that provides the quadratic friction, we find

$$\beta^{\text{Mont.}} \simeq \frac{\alpha_E\,\varphi^2}{d^2}\eta_f$$

Compared to our coefficient $\beta = \frac{150\varphi^2}{(1-\varphi)d^2}\eta_f$, a factor $(1-\varphi)$ is missing, but these expression can roughly coincide for values of α_E of the order of $150/(1-\varphi)$, even though the φ-dependency may be important.

S.A.5. *Energy balance of the depth-averaged model*

The energy balance of the system (2.16)-(2.26) is slightly modified from the original one presented in Bouchut et al. (2016), related to the boundary condition modification and reads

$$
\begin{aligned}
&\partial_t\Bigg(\rho_s\varphi h_m\tfrac{|\mathbf{v}|^2}{2}+\rho_f(1-\varphi)h_m\tfrac{|\mathbf{u}|^2}{2}+\rho_f h_f\tfrac{|\mathbf{u}_f|^2}{2}\\
&\quad+g\cos\theta\Big(\rho_s\varphi h_m+\rho_f((1-\varphi)h_m+h_f)\Big)(b+\tilde{b})\\
&\quad+(\rho_s-\rho_f)g\cos\theta\varphi\tfrac{h_m^2}{2}+\rho_f g\cos\theta\tfrac{(h_m+h_f)^2}{2}\Bigg)\\
&+\nabla\cdot\Bigg(\rho_s\varphi h_m\tfrac{|\mathbf{v}|^2}{2}\mathbf{v}+\rho_f(1-\varphi)h_m\tfrac{|\mathbf{u}|^2}{2}\mathbf{u}+\rho_f h_f\tfrac{|\mathbf{u}_f|^2}{2}\mathbf{u}_f\\
&\qquad+g\cos\theta\Big(\rho_s\varphi h_m\mathbf{v}+\rho_f((1-\varphi)h_m\mathbf{u}+h_f\mathbf{u_f})\Big)(b+\tilde{b}+h_m)\\
&\qquad+\rho_f g\cos\theta\Big(\varphi h_m\mathbf{v}+(1-\varphi)h_m\mathbf{u}+h_f\mathbf{u}_f\Big)h_f+(1-\varphi)h_m\overline{p^e_{f_m}}(\mathbf{u}-\mathbf{v})\Bigg)\\
&\leq\frac{1}{2}(\rho_s-\rho_f)\varphi g\cos\theta h_m^2\Phi+R_e-\frac{\delta_f}{2}|\mathbf{u}_f-\mathbf{u}|^2\rho_f|\mathcal{V}_f|\\
&\quad-\beta h_m|\mathbf{u}-\mathbf{v}|^2-|\mathbf{v}|\mu\left(\varphi(\rho_s-\rho_f)g\cos\theta h_m-(p^e_{f_m})_{|b}\right)-k_f|\mathbf{u}_f-\mathbf{v}_m|^2-\frac{5}{2}\frac{\eta_e(1-\varphi)}{h_m}|\mathbf{u}|^2,
\end{aligned}
\tag{S.A.26}
$$

with

$$
R_e=h_m\overline{p^e_{f_m}}\nabla\cdot\Big((1-\varphi)(\mathbf{u}-\mathbf{v})\Big)-(1-\varphi)(p^e_{f_m})_{|b}(\mathbf{u}-\mathbf{v})\cdot\nabla b.
$$

S.A.6. *Derivation of a pressure evolution equation*

In section 2.3.2 we introduced a new approach to solve the basal solid pressure for our depth-averaged model. The proposed equation is deduced from a 3-D evolution equation for the solid pressure that we derive from Baumgarten & Kamrin (2019). We give here the details of this approach. In this work the solid stress tensor $\sigma_s=-p_s\mathrm{Id}+\sigma_s'$ is solved through an evolution equation taking into account plastic effects (see equation 2.25 in Baumgarten & Kamrin (2019)). This equation reads†

$$
\partial_t\sigma_s+\mathbf{V}\cdot\nabla\sigma_s=2G\,D_{e0}+B\,\mathrm{tr}(D_e)\mathrm{Id}+W_s\sigma_s-\sigma_s W_s
$$

where G and B are the solid shear and bulk modulus respectively, $B=\frac{E}{3(1-2\nu)}, G=\frac{E}{2(1+\nu)}$ with E the Young's modulus and ν the Poisson's ratio. The solid strain rate $D(\mathbf{V})=\frac{1}{2}(\nabla\mathbf{V}+\nabla\mathbf{V}^t)$ is decomposed into an elastic strain rate D_e and a plastic contribution D_p, $D(\mathbf{V})=D_e+D_p$ with D_p given by

$$
D_p=\frac{\dot{\gamma}}{\sqrt{2}}\frac{\sigma_{s0}}{\|\sigma_{s0}\|}+\frac{1}{3}(\dot{\gamma}\tan\psi+\dot{\xi}_1+\dot{\xi}_2)\mathrm{Id}
$$

where σ_{s0} is the initial stress and $\dot{\xi}_1,\dot{\xi}_2$ are the rate of plastic expansion and compaction, respectively. D_{e0} represents the initial elastic strain rate. Finally, W_s is the rotational rate tensor (skew part of the velocity gradient), that is, $W_s=\frac{1}{2}(\nabla\mathbf{V}-\nabla\mathbf{V}^t)$.

The solid pressure is defined as $p_s=-\frac{1}{3}\mathrm{tr}(\sigma_s)$, so a transport equation for it may be

† For simplicity we will use the same gradient notation for 3-D and 2-D functions. It must be understood as $\nabla\mathbf{f}=(\partial_x\mathbf{f},\partial_y\mathbf{f},\partial_x\mathbf{f})$, for any function $\mathbf{f}(t,x,y,z)$, or as $\nabla f=(\partial_x f,\partial_y f)$ for any function $f(t,x,y)$.

deduced by taking the trace of the previous equation for σ_s. We neglect purely plastic effects, $\dot{\xi}_1 = \dot{\xi}_2 = 0$, and we assume a symmetric velocity gradient (symmetric solid plastic flow), $W_s = 0$. The equation for the solid pressure then reads

$$\partial_t p_s + \mathbf{V}\cdot\nabla p_s = -\frac{1}{3}(2G\,\mathrm{tr}(D_{e0}) + 3B\,\mathrm{tr}(D_e)).$$

Assuming that the solid phase begins in a stress-free state, $\sigma_{s0} = 0$, the plastic stress yields

$$D_p = \frac{1}{3}\dot{\gamma}\tan\psi\ \mathrm{Id}.$$

Then the trace of the elastic stress $D_e = D(\mathbf{V}) - D_p$ is

$$\mathrm{tr}(D_e) = \nabla\cdot\mathbf{V} - \dot{\gamma}\tan\psi.$$

If we assume that at the initial state the solid phase satisfies $\mathrm{tr}(D_{e0}) = 0$, what just means that the relation $\nabla\cdot\mathbf{V} = \dot{\gamma}\tan\psi$ is satisfied at the initial time, the pressure equation becomes

$$\partial_t p_s + \mathbf{V}\cdot\nabla p_s = -B(\nabla\cdot\mathbf{V} - \dot{\gamma}\tan\psi). \tag{S.A.27}$$

The equation (S.A.27) replaces the closure $\Phi = \dot{\gamma}\tan\psi$ in Bouchut et al. (2016) in the starting two-phase 3-D model given by the Jackson's equations. In order to obtain the depth-averaged model we must apply the shallow approximation and the depth-averaging process. Let us see in the next lines how to obtain (2.30) from (S.A.27). Firstly we remind that the 3-D velocity is denoted by $\mathbf{V}(t,x,y,z) = (\mathbf{v}^{\mathbf{x}}(t,x,y), v^z(t,x,y,z))$.
We first use $\nabla\cdot\mathbf{V} = \Phi$ to write $\partial_z v^z = \Phi - \nabla\cdot\mathbf{v}^{\mathbf{x}}$, then (S.A.27) yields

$$\partial_t p_s + \mathbf{v}^{\mathbf{x}}\cdot\nabla p_s + \partial_z(v^z p_s) = p_s(\Phi - \nabla\cdot\mathbf{v}^{\mathbf{x}}) - B(\Phi - \dot{\gamma}\tan\psi).$$

As in Bouchut et al. (2016), we use the approximations

$$\mathbf{v}^{\mathbf{x}} \sim \mathbf{v}+O(\epsilon^2),\quad \varphi \sim \bar{\varphi}+O(\epsilon^2),\quad \Phi \sim \bar{\Phi}+O(\epsilon^2),\quad \dot{\gamma} \sim \bar{\dot{\gamma}}+O(\epsilon^2),\quad \tan\psi \sim \tan\bar{\psi}+O(\epsilon^2),$$

to write

$$\partial_t p_s + \mathbf{v}\cdot\nabla p_s + \partial_z(v^z p_s) = p_s(\bar{\Phi} - \nabla\cdot\mathbf{v}) - B(\bar{\Phi} - \bar{\dot{\gamma}}\tan\bar{\psi}) + O(\epsilon^2). \tag{S.A.28}$$

Remind that here we denote $\mathbf{v} = \overline{\mathbf{v}^{\mathbf{x}}}$. We integrate this equation in $[b, b+h_m]$. Using

$$p_s = \bar{\varphi}(\rho_s - \rho_f)g\cos\theta(b + h_m - z) - p^e_{f_m}$$

we write

$$h_m\bar{p}_s \equiv \int_b^{b+h_m} p_s\,dz = \frac{h_m^2}{2}\bar{\varphi}(\rho_s - \rho_f)g\cos\theta - h_m\overline{p^e_{f_m}}$$

with $\overline{p^e_{f_m}} = \frac{1}{h_m}\int_b^{b+h_m} p^e_{f_m}\,dz$ and then $\bar{p}_s = \frac{h_m}{2}\bar{\varphi}(\rho_s - \rho_f)g\cos\theta - \overline{p^e_{f_m}}$. The integral of the left hand side of (S.A.28), using the Leibniz rule gives

$$\begin{aligned}
&\int_b^{b+h_m}(\partial_t p_s + \mathbf{v}\cdot\nabla p_s)\,dz + (v^z p_s)_{|b+h_m} - (v^z p_s)_{|b}\\
&= \partial_t(h_m\bar{p}_s) + \mathbf{v}\cdot\nabla(h_m\bar{p}_s) - p_s(b+h_m)(\partial_t(b+h_m) + \mathbf{v}\cdot\nabla(b+h_m) - v^z(b+h_m))\\
&+ p_s(b)(\partial_t b + \mathbf{v}\cdot\nabla b - v^z(b))\\
&= \partial_t(h_m\bar{p}_s) + \mathbf{v}\cdot\nabla(h_m\bar{p}_s).
\end{aligned}$$

In the last equality we used the definition of p_s and the boundary condition at the bottom that give $p_s(b+h_m) = 0$, and $v^z(b) = \mathbf{v}^{\mathbf{x}}{}_{|b}\cdot\nabla b \sim \mathbf{v}\cdot\nabla b$. From the mass equations we have

$$\partial_t h_m + \nabla\cdot(h_m\mathbf{v}) = h_m\bar{\Phi},$$

hence

$$\begin{aligned}\partial_t(h_m\bar{p}_s) + \mathbf{v}\cdot\nabla(h_m\bar{p}_s) &= h_m(\partial_t\bar{p}_s + \mathbf{v}\cdot\nabla\bar{p}_s) + \bar{p}_s(\partial_t h_m + \mathbf{v}\cdot\nabla h_m)\\ &= h_m(\partial_t\bar{p}_s + \mathbf{v}\cdot\nabla\bar{p}_s) + \bar{p}_s(h_m\bar{\Phi} - h_m\nabla\cdot\mathbf{v}).\end{aligned}$$

According to the asymptotic approximation, the second term on the right-hand side of the equation (S.A.28) does not depend on z up to ϵ^2, thus we obtain

$$h_m(\partial_t\bar{p}_s + \mathbf{v}\cdot\nabla\bar{p}_s) + \bar{p}_s h_m(\bar{\Phi} - \nabla\cdot\mathbf{v}) = h_m\bar{p}_s(\bar{\Phi} - \nabla\cdot\mathbf{v}) - Bh_m(\bar{\Phi} - \bar{\dot{\gamma}}\tan\bar{\psi}).$$

Then the depth-averaged equation for the averaged solid pressure writes

$$\partial_t\bar{p}_s + \mathbf{v}\cdot\nabla\bar{p}_s = -B(\bar{\Phi} - \bar{\dot{\gamma}}\tan\bar{\psi}). \tag{S.A.29}$$

We can write the basal solid pressure in terms of the averaged $\bar{p}_s$ as

$$p_{s\,|b} = h_m\bar{\varphi}(\rho_s - \rho_f)g\cos\theta - p^e_{f_m\,|b} = 2(\bar{p}_s + \overline{p^e_{f_m}}) - p^e_{f_m\,|b}.$$

This adds a new unknown $p^e_{f_m\,|b}$, but we can use the approximations found in Bouchut et al. (2016) to write $p^e_{f_m\,|b} = \frac{3}{2}\overline{p^e_{f_m}}$ and then, using again $\overline{p^e_{f_m}} = -\bar{p}_s + \frac{h_m}{2}\bar{\varphi}(\rho_s - \rho_f)g\cos\theta$ we write

$$p_{s\,|b} = 2\bar{p}_s - \frac{1}{2}\overline{p^e_{f_m}} = \frac{3}{2}\bar{p}_s - \frac{h_m}{4}\bar{\varphi}(\rho_s - \rho_f)g\cos\theta,$$

hence we find the relation between the basal and the averaged solid pressure,

$$\bar{p}_s = \frac{2}{3}p_{s\,|b} + \frac{h_m}{6}\bar{\varphi}(\rho_s - \rho_f)g\cos\theta.$$

We embed this relation in (S.A.29) to write the evolution equation for the basal solid pressure

$$\frac{2}{3}(\partial_t p_{s\,|b} + \mathbf{v}\cdot\nabla p_{s\,|b}) + \frac{1}{6}(\rho_s - \rho_f)g\cos\theta(\partial_t(h_m\bar{\varphi}) + \mathbf{v}\cdot\nabla(h_m\bar{\varphi})) = -B(\bar{\Phi} - \bar{\dot{\gamma}}\tan\bar{\psi}).$$

Therefore using (2.16*a*),

$$\partial_t p_{s\,|b} + \mathbf{v}\cdot\nabla p_{s\,|b} = \frac{1}{4}(\rho_s - \rho_f)g\cos\theta\bar{\varphi}h_m\nabla\cdot\mathbf{v} - \frac{3}{2}B(\bar{\Phi} - \bar{\dot{\gamma}}\tan\bar{\psi}). \tag{S.A.30}$$

The averaged excess pore pressure appearing in the system is recovered through

$$\overline{p^e_{f_m}} = \frac{2}{3}p^e_{f_m\,|b} = \frac{2}{3}(-p_{s\,|b} + h_m\bar{\varphi}(\rho_s - \rho_f)g\cos\theta).$$

Later in section S.B.1.2 we develop a comparison with the equation proposed in Iverson & George (2014) to solve the basal pressure.

Remark 3. *We would like to point out that equation (S.A.27) is obtained by neglecting the rates of plastic expansion and compaction $\dot{\xi}_1, \dot{\xi}_2$. As said in Baumgarten & Kamrin (2019) in most granular materials, the elastic deformation are extremely small compared to plastic deformation, the latter being even more important when the solid phase is flowing. Then our approximation (S.A.27) and the derived depth-averaged equation (2.30) are only valid when the elastic contribution is small (high solid bulk modulus B).*

Remark 4. *Other alternatives can be found in the literature where a pressure evolution equation taking into account dilatancy, is used to close the two-phase 3-D system. Let us mention the papers (Lee 2021; Montellà et al. 2021, 2023) where 3-D models are proposed to solve immersed granular flows. In Lee (2021) the following equation for the pressure is considered:*

$$\partial_t p_s + \mathbf{V}\cdot\nabla p_s = 2K\varphi\dot{\gamma}(p_s^{\mathrm{eq}} - p_s) - K_2\varphi\nabla\cdot\mathbf{V} - K_3 p_s\mathcal{H}(\varphi_0 - \varphi) \tag{S.A.31}$$

where the constants are: K (from the dilatancy law in Pailha & Pouliquen (2009), $\tan\psi = K(\varphi - \varphi^{eq})$), $K_3 = 100s^{-1}$, $\varphi_0 = 0.55$ (random loose packing), $\varphi_c = 0.576$,

$$K_2 = \begin{cases} a_e E & \varphi \geq \varphi_c \\ a_e E \frac{\varphi - \varphi_0}{\varphi_c - \varphi_0} & \varphi_0 \geq \varphi < \varphi_c \\ 0 & \varphi < \varphi_0 \end{cases}$$

with $a_e = 0.1$, and E is the Young modulus ($10^6 Pa$). The Heaviside function $\mathcal{H}(x)$ is 0 for negative values and 1 for positive or zero values.
As it was exposed in section 2.4 of Bouchut et al. (2016), for a linear approximation we can establish the following relation

$$K(\varphi - \varphi^{eq}) \sim K_p(p_s^{eq} - p_s),$$

and then the equation becomes

$$\partial_t p_s + \mathbf{V}\cdot\nabla p_s = -K_2\varphi\left(\nabla\cdot\mathbf{V} - \frac{2K}{K_2K_p}\dot{\gamma}(\varphi - \varphi^{eq})\right) - K_3 p_s \mathcal{H}(\varphi_0 - \varphi). \tag{S.A.32}$$

In the case $\varphi > \varphi_0$, the Heaviside function vanishes and this equation has the same form as the simplified equation from Baumgarten & Kamrin (2019), considered here in (S.A.27).
In Montellà et al. (2021) a simpler equation has been considered by taking

$$\partial_t p_s + \mathbf{V}\cdot\nabla p_s = K\varphi\dot{\gamma}(p_s^{eq} - p_s), \tag{S.A.33}$$

so only the first term in (S.A.31) is kept. Using the same approach, it can be written as

$$\partial_t p_s + \mathbf{V}\cdot\nabla p_s = -\frac{K}{K_p}\varphi\dot{\gamma}(\varphi - \varphi^{eq}). \tag{S.A.34}$$

The main difference is that this equation does not have the divergence term.

S.A.6.1. *Computation of the solid pressure at the bottom*

We compare here the two ways of calculating the basal solid pressure in the proposed models described in Section 2.3.2: either as the solution of the third-degree polynomial (2.28) or as the solution of the evolution equation (2.30) involving granular elasticity. For very large elastic solid bulk modulus, these equations are equivalent since (2.30) can be seen as a relaxation equation for the equation $\Phi = \dot{\gamma}\tan\psi$.

For this, we solve the full model (A1) with two layers and 3 velocities in the loose configuration with $C_h = 0.15$. For this value of C_h, the initial virtual thickness is $H^0 = 0.7762$ m, close to the mixture thickness $h_m^0 = 0.7169$ m (see section 5.2). We test several values of B, varying from 10^6 Pa to 10^9 Pa as a typical value for glass beads (Baumgarten & Kamrin 2019). In figure S6(left), we represent the normalized difference between the solution without elasticity and the solution accounting for grain elasticity $|p_{s_b}^{pol} - p_{s_b}^{eq}|$. The difference between the two calculations is non-negligible for $B = 10^6$ Pa (50%), lower for $B = 10^7$ Pa (10%) and drops below 0.1% for $B = 10^9$ Pa. We also tested the value $B = 10^5$ Pa and the difference is greater than 50%. Note that these values occur at the beginning of the simulation ($t = 0.1$ s). After that, they are much smaller, less than 1% for the $B = 10^6$ Pa case. Figure S6(right) shows that for $B > 10^6$ Pa, the effect of elasticity on the basal excess pore pressure is very small and the difference in the solution of the pressure is not noticeable. As pointed out in remark 3 in section S.A.6, equation (2.30) is only valid for a small contribution of elastic effects. Otherwise, plastic expansion and contraction rates must be considered in the model. Thus, for the configuration here, the use of (2.30) to solve the solid pressure remains valid only for $B \leq 10^6$. Note that this value holds for several granular mixtures such as glass beads

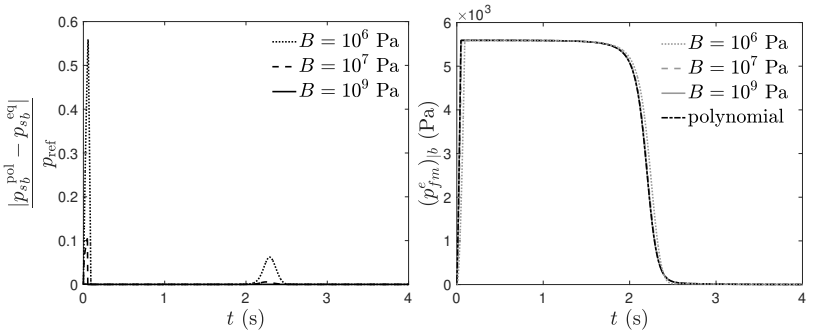

Figure S6: Values obtained for model (A1) [2L: $(u,v)\,|\,u_f$] for several values of the coefficient B. Left: Normalized absolute error obtained with the two options of computing basal solid pressure: $p_{s_b}^{\mathrm{pol}}$ denotes the solution obtained when using the polynomial and $p_{s_b}^{\mathrm{eq}}$ when using the relaxation equation. The reference pressure p_{ref} is the maximum of the solution $p_{s_b}^{\mathrm{pol}}$. Right: corresponding basal excess pore pressure $p_{f_m\,|b}^e$ obtained using equation (2.30).

or sand-gravel. The elasto-plastic effects in debris flows models need further investigation that is outside the scope of this study. Nevertheless, the proposed evolution equation (2.30) provides an interesting alternative to compute the basal pressure, mainly from the numerical point of view as a relaxation equation for the dilatancy law, and is thus more suitable for more complex models, such as multilayer models, as discussed in section 2.3.2.

As discussed above, the same type of equation was proposed in the Iverson-George model to calculate the basal fluid pressure (see equation (3.17*d*)). In their equation $B = 1/\alpha$, where α is the elastic compressibility, that varies between $10^{-7} - 10^{-2}$ Pa^{-1}. Indeed, as described in detail in Iverson & George (2014), nearly liquefied debris-flow slurries with $\varphi \geq 0.4$ generally exhibits behavior consistent with $\alpha \sim 10^{-5}$ Pa^{-1}. Compressibilities as large as $\alpha \sim 10^{-2}$ Pa^{-1} are found for relatively dilute, mud-rich slurries and dredged sludges with $p_{s_b} < 10^3$ Pa and $\varphi < 0.4$, whereas values of $\alpha \sim 10^{-7}$ Pa^{-1} are more appropriate for loosely packed sand and sand-gravel mixtures. Iverson & George (2014) proposed the empirical relation (see their equation 3.14)

$$\alpha = \frac{a}{\varphi(p_{s_b} - \sigma_0)} \tag{S.A.35}$$

where a is a proportionality calibration coefficient ($a \sim 0.01 - 0.05$) and σ_0 a reference stress ($\sigma_0 \sim 10 - 1000$ Pa). In the uniform configuration solved in this paper, for $\sigma_0 = 1000$ Pa (typical for debris used in flume experiments), these values of a give $B \sim 10^5$. As shown above, this value is not small enough to neglect the elasticity in the model. We would have to decrease a to 10^{-3} to obtain $B \sim 10^7$.

S.B. Comparison with the Iverson-George model and the Meng-Wang model: further details

S.B.1. *Comparison with the Iverson-George model*

S.B.1.1. *Details of calculations*

We claimed that the Iverson-George model is equivalent to our oversimplified mixture model (C2) (equations (3.13)) which has been deduced from our two-layer mixture model (B2) (equations (3.2)) under the hypothesis $\Delta_H \ll 1$. In this section we detail the comparison

between (3.2) and the Iverson-George model (3.17) as well as the hypotheses making it possible to recover the Iverson-George model from our model.

In view of the conservation laws (3.17*b*) and (3.2*a*), we see that the virtual thickness h in the Iverson-George model corresponds to our H. From (3.2*a*) and (3.4) (or equivalently (2.27)) we obtain the continuity equation for the virtual thickness H since

$$\partial_t H + \nabla \cdot (H\mathbf{v}) = \frac{\rho - \rho_f}{\rho} H\Phi.$$

This equation coincides with equation (3.17*a*) in the Iverson-George model when

$$D = h\Phi,$$

as claimed in (3.22). Our equation for the upper fluid layer thickness (3.2*b*) obviously does not appear in the Iverson-George model.

Then we have to compare the momentum equations (3.8*d*) and (3.17*c*). Instead of the equation (3.17*c*) on $h\mathbf{v}$, let us write it on $\rho h\mathbf{v}$

$$\begin{aligned}\partial_t(\rho h\mathbf{v}) + \nabla \cdot (\rho h\mathbf{v} \otimes \mathbf{v}) + \kappa g \cos\theta \nabla \left(\frac{1}{2}\rho h^2\right) + \kappa g \cos\theta \frac{h^2}{2}\nabla\rho + h(1-\kappa)\nabla p_b \\ = -\rho h g \cos\theta \nabla b - \rho g h \sin\theta \mathbf{e}_x - \mu_{\mathrm{IG}} \operatorname{sgn}(v)(\rho g \cos\theta h - p_b) - \frac{2\eta_e}{h}(1-\varphi)\mathbf{v},\end{aligned} \tag{S.B.1}$$

where we replaced τ_s and τ_f using (3.18*a*). We rewrite (3.8*d*) here using (3.10)-(3.11) to make the comparison easier:

$$\begin{aligned}&\partial_t(\rho H\mathbf{v}) + \nabla \cdot (\rho H\mathbf{v} \otimes \mathbf{v}) + g\cos\theta\nabla\left(\frac{1}{2}\rho\Big(H^2 + \frac{\rho-\rho_f}{\rho_f}\Delta_H^2\Big)\right) \\ &= -\rho H g\cos\theta\nabla b - \rho H g \sin\theta \mathbf{e}_x - \mu \operatorname{sgn}(\mathbf{v})\ \big(\rho g\cos\theta H - (p_{f_m})_{|b}\big) - \frac{5}{2}\frac{\eta_e(1-\varphi)}{H-\Delta_H}\mathbf{v}.\end{aligned} \tag{S.B.2}$$

Firstly, we notice that the term $\kappa g \cos\theta \frac{h^2}{2}\nabla\rho$ in (S.B.1) does not appear in (S.B.2). This term can be neglected in the model as the authors argue in George & Iverson (2014) under the assumption of small gradient in ρ. Secondly, in order to make these momentum equations look the same, we have to set $\kappa = 1$, that is, we assume isotropy of normal stresses. Notice that the convective terms are the same in the two models with $h = H$ but it is not the case for the pressure terms and the basal shear for the fluid. Under the condition

$$\Delta_H = H - h_m \ll H \tag{S.B.3}$$

the pressure term $g\cos\theta\nabla(\rho h^2/2)$ in (S.B.1) identifies with the equivalent pressure term in (S.B.2) and the shear term becomes the same, $\frac{2\eta_e(1-\varphi)}{H}$, except for the coefficient coming from the approximation of the strain shear rate, 2 for the Iverson-George model and 5/2 for our model.

We now focus on the friction term at the bottom which involves the basal pressure and the friction coefficient $\mu = (\mu^{\mathrm{eq}} + \tan\psi)_+$ for us and $\mu_{\mathrm{IG}} = \tan(\delta + \psi_{\mathrm{IG}})$ in the Iverson-George model. Assuming a linearization of the tangent, we write

$$\mu_{\mathrm{IG}} \simeq \tan\delta + \tan\psi_{\mathrm{IG}}.$$

As we said in section 3.4.2, the main difference is that the friction coefficient in the critical state $\mu_c = \tan\delta$ is thus constant while it depends on the inertial and viscous numbers in our model $\mu^{\mathrm{eq}}(\mathcal{J}_\mu)$ (see equations (2.10) and (2.15)). We would like to make a more detailed analysis of the rheology: for us it is given by (2.12), (2.10) and for Iverson-George by (3.18*e*).

An explicit comparison has been summarized in table 3. The form of the dimensionless parameter N in (3.18*e*) is obtained as a generalization of the viscous number $J = \frac{\eta_f \dot{\gamma}}{\sigma_e}$ taking into account a collision term $\rho_s d^2 \dot{\gamma}^2$, that helps to avoid the division by zero in case of vanishing pressure σ_e, that is

$$N = \frac{\eta_e \dot{\gamma}}{\sigma_e + \rho_s d^2 \dot{\gamma}^2}.$$

Notice that in this definition the fluid viscosity η_f in J has been replaced by the effective shear viscosity η_e, even if later in the paper Iverson & George (2014) it is assumed as a constant, considering the pore fluid as a Newtonian viscous material. Dividing by the pressure σ_e we find the inertial number I^2 in the denominator of N as shown in (3.18*e*). In our model we do not consider the collision term but a combined inertial-viscous number $\mathcal{J}_\varphi$. Notice that the approximation of the shear rate $\dot{\gamma}$ also differs, given by (2.13) and (3.18*d*), respectively. The coefficient 2 in (3.18*d*) is related to a particular shape of the velocity profile. Indeed, the detailed study of Cassar et al. (2005) shows that a coefficient 3 corresponds to the viscous regime (used for example in Pailha & Pouliquen (2009)) and a more general coefficient 5/2 is compatible with the free fall or inertial regimes (used for example in Bouchut et al. (2021)), which is also the choice made here (2.13). Beside the coefficient, in our approximation it is the thickness of the mixture which is involved in the shear rate and not the virtual thickness H as discussed in Section 3.3.

The basal pressure in the Coulomb law is represented by σ_e in the Iverson-George model (3.18*a*) and by $p_{s\,|b}$ for us (3.10)

$$\sigma_e = \rho g \cos\theta h - p_b, \qquad p_{s\,|b} = \rho g \cos\theta H - (p_{f_m})_{|b}.$$

If we assume $h = H$, the hydrostatic contribution is the same in the two models. In the Iverson-George model the basal excess fluid pressure p_b is the solution of equation (3.17*d*). If we assume $\alpha \to 0$, this equation reduces to

$$D = 2|\mathbf{v}|\tan\psi_{\mathrm{IG}}, \tag{S.B.4}$$

and the pressure p_b, obtained in the Iverson-George model by inverting (3.18*c*), is

$$p_b = \rho_f g \cos\theta h - \frac{\eta_e}{2k_{\mathrm{IG}}} hD. \tag{S.B.5}$$

By considering (3.22) we can write

$$p_b = \rho_f g \cos\theta h - \frac{\eta_e}{2k_{\mathrm{IG}}} h^2 \Phi. \tag{S.B.6}$$

In our model the basal excess fluid pressure is given in equation (3.11)

$$(p_{f_m})_{|b} = \rho_f g \cos\theta \left(H + \frac{\rho - \rho_f}{\rho_f} \Delta_H \right) + (p^e_{f_m})_{|b}.$$

The hydrostatic part would then coincide under (S.B.3). Now we have to compare the last term coming from the excess pore pressure, that reads $-\frac{\eta_e}{2k_{\mathrm{IG}}} h^2 \Phi$ for the Iverson-George model and $(p^e_{f_m})_{|b}$ for our model. According to (3.9*a*) and to the value of β in (2.21),

$$(p^e_{f_m})_{|b} = -\frac{\eta_f}{k} \frac{h_m^2}{2} \Phi = -\frac{\eta_f}{k} \frac{(H - \Delta_H)^2}{2} \Phi, \tag{S.B.7}$$

and then both definitions are the same under (S.B.3) for k and k_{IG} denoting both the hydraulic permeability, calculated differently in the two models in (2.21) and (3.18*c*) respectively, and assuming a constant effective fluid viscosity $\eta_e = \eta_f$.

We conclude that the limit $\alpha \to 0$ in the Iverson-George model with $\kappa = 1$ and neglecting the term $g \cos\theta \frac{h^2}{2} \nabla\rho$ in (S.B.1) can be considered as a simplification of our one velocity two-layer (3.2) under the assumption (S.B.3) and with $h = H$. In these conditions, the Iverson-George model corresponds to our one-layer model one-velocity model (3.13).

S.B.1.2. *Comparison of the basal pore pressure equation*

We compare here the equations for the solid basal pressure proposed in this paper (2.30) and in the Iverson-George model (3.17*d*). First let us briefly remind how equation (3.17*d*) is obtained in the Iverson-George model, from a Darcy law and dilatancy relations, following Iverson & George (2014). The same notation as in section S.A.6 is used here, namely, 3-D velocity is denoted by $\mathbf{V}(t,x,y,z) = (\mathbf{v}^{\mathbf{x}}(t,x,y), v^z(t,x,y,z))$ and the same gradient notation is used for both, 3-D and 2-D functions. Moreover the material derivative is $D_t(\xi) = \partial_t\xi + \mathbf{V}\cdot\nabla\xi$, for any function ξ. In particular, the 3-D dilatancy law is given by

$$\dot\gamma \tan\psi_{\rm IG} = \alpha D_t\sigma_e - \frac{1}{\varphi} D_t\varphi$$

where the first term on the r.h.s. accounts for the elasticity effect. The evolution of the volume fraction, appearing in the last term, is related to the divergence of the solid velocity and the apparent fluid velocity $\mathbf{Q} = (1-\varphi)(\mathbf{U}-\mathbf{V})$ through the relation,

$$\frac{1}{\varphi} D_t\varphi = -\nabla\cdot\mathbf{V} = \nabla\cdot\mathbf{Q}.$$

The dilatancy law then reads as in (2.29)

$$\alpha D_t\sigma_e = -\nabla\cdot\mathbf{V} + \dot\gamma\tan\psi_{\rm IG}, \tag{S.B.8}$$

when $\alpha = 1/B$. The Darcy law is given by

$$\mathbf{Q} = -\frac{k_{\rm IG}}{\eta_e}\nabla p_e.$$

Considering that the mean total normal stress is defined as $\sigma = p_f + \sigma_e$, combining these equations leads to

$$\alpha D_t(p_f - \sigma) = \nabla\cdot\left(\frac{k_{\rm IG}}{\eta_e}\nabla p_e\right) - \dot\gamma\tan\psi_{\rm IG},$$

In depth-averaging this equation, several hypothesis are considered to finally achieve (3.17*d*) as summarized in the following lines

- Shallow flow assumption is considered and the equation is approximated at first order in $\epsilon = H/L$,

$$\alpha D_t(p_f - \sigma) = \partial_z\left(\frac{k_{\rm IG}}{\eta_e}\partial_z p_e\right) - \dot\gamma\tan\psi_{\rm IG}.$$

- $\dfrac{k_{\rm IG}}{\eta_e}$ does not depend on z (no material property varies in z). Notice that since $p_f = p_h + p_e$ and $p_h = \rho_f g\cos\theta(h-z)$, we have $\partial_z^2 p_e = \partial_z^2 p_f$. Then

$$\alpha D_t(p_f - \sigma) = \frac{k_{\rm IG}}{\eta_e}\partial_z^2 p_f - \dot\gamma\tan\psi_{\rm IG}.$$

- A linear profile in z is assumed for the vertical velocity. Using $v^z(z=0) = 0$ and the kinematic condition $v^z(z=h) = \partial_t h + \mathbf{v}^{\mathbf{x}}\cdot\nabla h$, then v^z is approximated by $v^z = \dfrac{z}{h}\bar D_t h$, with

$\bar{D}_t h = \partial_t h + \mathbf{v}\cdot\nabla h$. As a consequence, $D_t(\xi) \sim \bar{D}_t(\xi) + \frac{z}{h}\bar{D}_t h\, \partial_z(\xi)$. The equation becomes,

$$\alpha\left(\bar{D}_t(p_f - \sigma) + \frac{z}{h}\bar{D}_t h\, \partial_z(p_f - \sigma)\right) = \frac{k_{\mathrm{IG}}}{\eta_e}\partial_z^2 p_f - \dot{\gamma}\tan\psi_{\mathrm{IG}}.$$

- Boundary conditions for the pressure: At the free surface, traction free for solid and fluid phases are considered, $p_{f\,|z=h} = \sigma_{e\,|z=h} = 0$. At the bottom, hydrostatic pore pressure gradient is assumed, $\partial_z p_{f\,|z=0} = -\rho_f g\cos\theta$. The depth-averaging of previous equation yields

$$\alpha h\bar{D}_t(\bar{p}_f - \bar{\sigma}) = \frac{k_{\mathrm{IG}}}{\eta_e}(\partial_z p_{f\,|z=h} + \rho_f g\cos\theta) - h\bar{\dot{\gamma}}\tan\bar{\psi}_{\mathrm{IG}},$$

where for clarity in the exposition we used the "overline" notation for the depth-averaged quantities, that is, for any f, $\bar{f} = \frac{1}{h}\int_0^h f dz$. It is assumed that α is constant in z, $\mathbf{v}^{\mathbf{x}} \sim \mathbf{v}$, $\bar{\dot{\gamma}} \sim \dot{\gamma}_{\mathrm{IG}} = \frac{2|\bar{\mathbf{v}}|}{h}$, $\tan\bar{\psi}_{\mathrm{IG}}$ is defined as in (3.18*e*) for $\bar{\varphi}$.

- A quadratic profile in z is specified for the pore fluid pressure, $\partial_z^2 p_f = C$ (cst. in z), that thanks to previous boundary condition gives

$$p_f = p_b\left(1 - \frac{z^2}{h^2}\right) - \rho_f g\cos\theta h\left(\frac{z}{h} - \frac{z^2}{h^2}\right).$$

This expression is used to find $\bar{p}_f$ and $\partial_z p_{f\,|z=h}$ to be replaced in the pressure equation, leading to

$$\alpha h\bar{D}_t\left(\frac{2}{3}p_b - \frac{1}{6}\rho_f g\cos\theta h - \bar{\sigma}\right) = \frac{k_{\mathrm{IG}}}{\eta_e}\left(\rho_f g\cos\theta - 2\frac{p_b}{h} + \rho_f g\cos\theta\right) - h\bar{\dot{\gamma}}\tan\bar{\psi}_{\mathrm{IG}}.$$

- Depth-averaged total normal stress is defined as $\bar{\sigma} = \frac{1}{2}\rho g\cos\theta h$ (half of the basal total normal traction). The equation becomes

$$\alpha h\bar{D}_t\left(\frac{2}{3}p_b - \frac{1}{2}g\cos\theta h\left(\frac{1}{3}\rho_f + \rho\right)\right) = \frac{2k_{\mathrm{IG}}}{\eta_e}\left(\rho_f g\cos\theta - \frac{p_b}{h}\right) - h\bar{\dot{\gamma}}\tan\bar{\psi}_{\mathrm{IG}},$$

and developing the first term,

$$\frac{2}{3}\alpha h\bar{D}_t p_b - \frac{1}{2}\alpha h g\cos\theta\left(\frac{1}{3}\rho_f\bar{D}_t h + \bar{D}_t(\rho h)\right) = \frac{2k_{\mathrm{IG}}}{\eta_e}\left(\rho_f g\cos\theta - \frac{p_b}{h}\right) - h\bar{\dot{\gamma}}\tan\bar{\psi}_{\mathrm{IG}}.$$

Mass equations (4.5 and 4.6 in Iverson & George (2014)) give respectively $\bar{D}_t(\rho h) = -\rho h\nabla\cdot\mathbf{v}$ and $\bar{D}_t h = \frac{\rho-\rho_f}{\rho}D - h\nabla\cdot\mathbf{v}$.
Embedding these expressions in the previous equation, we finally write the pressure equation as

$$\bar{D}_t p_b + \frac{1}{4}g\cos\theta\left((\rho_f + 3\rho)h\nabla\cdot\mathbf{v} - \rho_f\frac{\rho-\rho_f}{\rho}D\right) = \frac{3}{2\alpha}\left(\frac{2k_{\mathrm{IG}}}{\eta_e h^2}\left(\rho_f g\cos\theta h - p_b\right) - \bar{\dot{\gamma}}\tan\bar{\psi}_{\mathrm{IG}}\right).$$

Using expressions (3.18*b*) and (3.18*c*) in the first term on the r.h.s. we find (3.17*d*),

$$\partial_t p_b + \mathbf{v}\cdot\nabla p_b = -\frac{1}{4}g\cos\theta\left((\rho_f + 3\rho)h\nabla\cdot\mathbf{v} - \rho_f\frac{\rho-\rho_f}{\rho}D\right) + \frac{3}{2\alpha}\left(\frac{D}{h} - \bar{\dot{\gamma}}\tan\bar{\psi}\right). \quad \text{(S.B.9)}$$

To derive the expression of the dilatancy term D in (3.18*c*), defined as $D = \int_0^h \nabla\cdot\mathbf{V}dz$, one uses again the hypothesis above. Namely, thanks to the dilatancy relations,

$$D = \int_0^h \nabla\cdot\mathbf{V}dz = \int_0^h \nabla\cdot\left(\frac{k_{\mathrm{IG}}}{\eta_e}\nabla p_e\right)dz \sim \int_0^h \frac{k_{\mathrm{IG}}}{\eta_e}\partial_z^2 p_f\, dz.$$

where we used the shallow approximation, that $\frac{k_{\rm IG}}{\eta_e}$ does not depend on z and $\partial_z^2 p_e = \partial_z^2 p_f$. Finally, the quadratic profile of p_f gives $\partial_z^2 p_f = \frac{2}{h^2}(\rho_f g\cos\theta h - p_b)$, so

$$D = \frac{2k_{\rm IG}}{\eta_e h}(\rho_f g\cos\theta h - p_b).$$

Note that thanks to the expression of the basal fluid pressure (3.18*b*), the equation (S.B.9) can be written as an equation for the excess pore-pressure p_e. This evolution equation implies a relaxation of the dilatancy law, and then a no direct vanishing of the excess pore pressure when $\varphi = \varphi^{\rm eq}$ is obtained as for our closure equation. If we look for a quasi-static solution of the pressure evolution equation of the Iverson-George model, the next solution is found (see equation 6.3 in Iverson & George (2014))

$$p_e = p_e(0)e^{-\delta t}, \quad \text{with} \quad \delta = \frac{k_{IG}}{\eta_f h}\left(\frac{3}{\alpha h} + \frac{1}{2}g\cos\theta\rho_f\frac{\rho-\rho_f}{\rho}\right).$$

Notice that the same solution is obtained for the uniform case studied in the presented manuscript. This expression tells that the relaxation of the excess pore pressure depends on the values of the permeability, viscosities and coefficient α. For the values considered in the numerical test performed in our work, the relaxation coefficient in the expression above gives $\delta \sim 17,92$. Thus the basal pore-pressure relaxation time is $\delta^{-1} \sim 0.055$ so we are not able to see a smooth decay of the pore-pressure and it becomes of the order of 10^{-12} when φ reaches $\varphi^{\rm eq}$.

Comparison with our proposal (2.30)

Firstly we remark that the 3-D equations for the pressure are the same in both models, (2.29) for our model and (S.B.8) for the Iverson-George model, under $\alpha = 1/B$. However the depth-averaging process is developed differently. We compare here the resulting depth-averaged equations, (2.30) and (3.17*d*). We drop the overline notation for simplicity.

Notice that in the Iverson-George model the evolution equation is established for the basal fluid pressure, while our proposal (2.30), developed in section S.A.6, is derived for the basal solid pressure. Let us then write our equation (S.A.30) in terms of the fluid pressure by using the relation $p_{s\,|b} = -p_{f_m\,|b} + g\cos\theta(\rho_f h_f + \rho h_m)$. First we compute the following transport term by using mass equations (2.16) and (2.25).

$$\begin{aligned}
&\partial_t(\rho_f h_f + \rho h_m) + \mathbf{v}\cdot\nabla(\rho_f h_f + \rho h_m)\\
&\quad = \partial_t(\rho_f h_f + \rho h_m) + \nabla\cdot((\rho_f h_f + \rho h_m)\mathbf{v}) - (\rho_f h_f + \rho h_m)\nabla\cdot\mathbf{v}\\
&\quad = \rho_f(\mathcal{V}_f - h_f\nabla\cdot\mathbf{v}) + \nabla\cdot(\rho_f h_f(\mathbf{v}-\mathbf{u}_f)) + \rho_f h_m\Phi - \rho h_m\nabla\cdot\mathbf{v}\\
&\quad = -(\rho_f h_f + \rho h_m)\nabla\cdot\mathbf{v} + \rho_f\nabla\cdot((1-\varphi)h_m(\mathbf{v}-\mathbf{u}) + h_f(\mathbf{v}-\mathbf{u}_f)).
\end{aligned}$$

The equation (2.30) reads

$$\begin{aligned}
\partial_t p_{f_m\,|b} + \mathbf{v}\cdot\nabla p_{f_m\,|b} = &-\frac{1}{4}g\cos\theta((5\rho-\rho_f)h_m + 4\rho_f h_f)\nabla\cdot\mathbf{v} + \frac{3}{2}B(\Phi - \dot\gamma\tan\psi)\\
&+\rho_f g\cos\theta\nabla\cdot\Big((1-\varphi)h_m(\mathbf{v}-\mathbf{u}) + h_f(\mathbf{v}-\mathbf{u}_f)\Big).
\end{aligned} \tag{S.B.10}$$

Let us compare equations (S.B.9) and (S.B.10) under $\alpha = 1/B$ and $D = h\Phi$. Notice that for a unique velocity $\mathbf{u} = \mathbf{v} = \mathbf{u}_f$ the last term in (S.B.10) vanishes. The additional term in the Iverson-George model equation (S.B.9) related to D, $\frac{1}{4}g\cos\theta\rho_f\frac{\rho-\rho_f}{\rho}D$, comes from the mass equations written in terms of the virtual surface – equations (4.5) and (4.6) in Iverson

& George (2014)– that read

$$\partial_t(\rho h) + \nabla\cdot(\rho h\mathbf{v}) = 0, \qquad \partial_t h + \nabla\cdot(h\mathbf{v}) = \frac{\rho-\rho_f}{\rho}D.$$

These equations are used during the integration procedure providing the additional term in the Iverson-George model equation (S.B.9). In our case the depth-averaging is made in $[0, h_m]$ instead of $[0, H]$, so we use the corresponding mass equation ,

$$\partial_t h_m + \nabla\cdot(h_m\mathbf{v}) = h_m\Phi.$$

Finally, the different coefficients of the densities that go with $\nabla\cdot\mathbf{v}$ in the first term on the r.h.s., come from the particular parabolic profile of the pressure assumed in Iverson & George (2014), as shown above. The corresponding term in (S.B.10) is also written as

$$-\frac{1}{4}g\cos\theta((5\rho-\rho_f)H-(\rho-\rho_f)\Delta_H)\nabla\cdot\mathbf{v}$$

so even neglecting Δ_H these coefficients do not coincide.

S.B.2. *Comparison with the Meng-Wang model*

S.B.2.1. *Details of calculations*

In section 4.3.2 we summarized the hypothesis under which the Meng-Wang model becomes our model (C1). Here we give a detailed explanation of this comparison in order to conclude that the equivalence is achieved under condition (3.12), $\Delta_H \ll 1$, as for the Iverson-George model.

The total mass conservation is given in (4.3) for our model and, for the Meng-Wang model it is obtained as the sum of the mass equations in (4.11)

$$\partial_t(\rho h) + \nabla\cdot(\rho h\mathbf{v}_m) = 0.$$

This leads to the same conclusion than for the Iverson-George model, that is, the equivalence between the virtual surface h and our virtual thickness H. Under this identification we recover the equivalence of the mass equations of the two systems (4.4*a*), (4.4*b*) and (4.11*b*), (4.11*a*) with $\mathfrak{I}$ in (4.11*f*), bridging the difference between the dilatancy laws. The equation of the upper fluid layer is neglected under (3.12) which also implies that $\mathcal{V}_f \ll 1$. But contrarily to the Iverson-George model case, this assumption not only implies $|\Phi|\ll 1$, but also that $\|\mathbf{u}-\mathbf{v}\|\ll 1$ from the definition of $\mathcal{V}_f$ in (4.4*f*). As in the precedent case, we will keep however this effect in the system, together with two different velocities. Under $\Delta_H \ll 1$, we find the following equivalence between $\mathfrak{I}$ and $\mathcal{V}_f$,

$$\mathfrak{I} = \varphi\frac{\rho_f\rho_s}{\rho}\mathcal{V}_f \simeq \varphi\frac{\rho_f\rho_s}{\rho}\mathcal{V}_f^*. \tag{S.B.11}$$

with $\mathcal{V}_f^*$ in (4.9).

Now we compare the momentum equations. Since we do not kept the viscous terms in the stress tensor, we must neglect the last term in (4.11*d*). We notice that $h = H$ is not enough to obtain the equivalence of the convective terms, and we must use again (3.12). We look carefully at the rest of the terms: pressure, mass exchange and friction.

Let us start with the pressure terms. Under $b = 0$, the equivalence of the hydrostatic pressure terms is found under (3.12). Regarding the excess pore pressure terms, in the solid and fluid equations it appears

$$\begin{array}{ll}\text{for Meng-Wang (4.11):} & (1-\varphi)\nabla(hp_e),\\ \text{for our model (4.4):} & (1-\varphi)(H-\Delta_H)\overline{\nabla p^e_{f_m}},\end{array}$$

where $\overline{\nabla p^e_{f_m}}$ is given by (2.20). Notice that p_e and $\overline{p^e_{f_m}}$ represent the depth-averaged excess pore pressures for each model. We will consider the capital notation for the z-dependent pressures in this section to avoid confusion. From the definition of these averages we have $\nabla(hp_e) = \nabla\Big(\int_b^{b+h} P_e\Big)$ and

$$\overline{\nabla p^e_{f_m}} = \frac{1}{h_m}\int_b^{b+h_m} \nabla P^e_{f_m} = \frac{1}{h_m}\left(\nabla\int_b^{b+h_m} P^e_{f_m} - (P^e_{f_m})_{|b+h_m}\nabla(b+h_m) + (P^e_{f_m})_{|b}\nabla b\right),$$

which gives (2.20*a*) since $(P^e_{f_m})_{|b+h_m} = 0$ from its definition (2.33). Using that $h_m = H - \Delta_H$, both expressions coincide in the case $b = 0$ and $\Delta_H \ll 1$. Despite the equivalence of the definitions, the approximations of the pore pressure given by (4.11*i*) for the Meng-Wang model and (2.20) for our model, differs in the explicit quantities:

$$\begin{aligned}
&\text{for Meng-Wang:} && \nabla(hp_e) = \nabla\left(-\tfrac{h^3}{3}\tfrac{\beta}{(1-\varphi)^2}\Big(\Phi_{\mathrm{MW}} + \nabla((1-\varphi)(\mathbf{u}-\mathbf{v}))\Big)\right),\\
&\text{for our model:} && (H-\Delta_H)\overline{\nabla p^e_{f_m}} = \nabla\left(-\tfrac{(H-\Delta_H)^3}{3}\tfrac{\beta}{(1-\varphi)^2}\Phi\right).
\end{aligned}$$

Indeed the term appearing in the Meng-Wang model corresponds to the case of $\beta \sim O(1)$ studied in Bouchut et al. (2016), where the values of $\overline{p^e_{f_m}}$ and $(p^e_{f_m})_{|b}$ are given in equations (3.58)-(3.59) of that paper matching with (4.11*i*) for $b = 0$.
Let us continue with the mass exchange term that reads

$$\begin{aligned}
&\text{for Meng-Wang (4.11):} && ((1-\lambda)\mathbf{u} + \lambda\mathbf{v})\mathfrak{I},\\
&\text{for our model (4.4):} && \tfrac{\rho_s\varphi}{\rho}((1-\lambda_f)\mathbf{u} + \lambda_f\mathbf{v}_m)\rho_f\mathcal{V}_f.
\end{aligned}$$

Assuming the equivalence in (S.B.11), and again $\Delta_H \ll 1$ a simple calculation leads to match

$$\lambda = \frac{\varphi\rho_s}{\rho}\lambda_f \simeq \frac{\varphi\rho_s}{\rho}\lambda_f^*. \tag{S.B.12}$$

There are three friction terms. The one with the relative velocity, $\beta(\mathbf{u}-\mathbf{v})$, is equivalent under $h = H$. The basal solid friction reads

$$\begin{aligned}
&\text{for Meng-Wang (4.11):} && -\operatorname{sgn}(\mathbf{v})\mu_{\mathrm{MW}}\Big(\varphi(\rho_s-\rho_f)hg\cos\theta - (p_e)_{|b}\Big) - \alpha_s\varphi\mathbf{v}\\
&\text{for our model (4.4):} && -\operatorname{sgn}(\mathbf{v})\mu\left(\varphi(\rho_s-\rho_f)g\cos\theta(H-\Delta_H) - (p^e_{f_m})_{|b}\right)
\end{aligned}$$

and the basal fluid friction,

$$\begin{aligned}
&\text{for Meng-Wang (4.11):} && -\alpha_f(1-\varphi)\mathbf{u},\\
&\text{for our model (4.4):} && -\tfrac{5}{2}\tfrac{\eta_e(1-\varphi)}{h_m}\mathbf{u}.
\end{aligned}$$

Thus it is easy to conclude that for a complete equivalence α_s must vanish and $\alpha_f = \frac{5}{2}\frac{\eta_e}{h_m}$. The difference in the approximation of the excess pore pressure indicated before also affects the Coulomb friction term. The remaining differing terms appearing in our model (4.4) are the last ones in momentum equations that are neglected again under $\Delta_H \ll 1$.

Therefore, as for the Iverson-George model the equivalence $h \simeq H$ and the condition (3.12) are needed to identify the systems.

S.B.2.2. *Comparison of the boundary conditions*

As discussed in Section 4.3, the Meng-Wang model is a depth-averaged model based on the 3-D Jackson's equations. The concept of the virtual surface, introduced by Iverson and George (Iverson & George 2014), is used to derive the model, thereby the real free surface is not solved. In contrast to the Iverson-George model, the Meng-Wang model solves for

two velocities, one for each phase (as in our (C1) model, see figure 3**C1**). Additionally, the flux of granular or liquid mass through the virtual surface is quantified in the model through specific boundary conditions at the virtual surface level. Since this is not a trivial matter, we present here the boundary conditions considered in Meng & Wang (2018) and highlight the main similarities and differences with respect to the ones considered for our model, in Section S.A.1. Note that in our case the configuration is different because instead of the virtual surface, we have the free surface $b + h_m + h_f$ and the interface $b + h_m$ that separate the mixture layer from the upper fluid layer (see figure 1).

The virtual surface in the Meng-Wang model is driven following the mixture velocity through the kinematic condition

$$\partial_t(b + h) + \mathbf{V}_m \cdot \mathbf{N}_X^{vs} = 0, \tag{S.B.13}$$

where $\mathbf{N}_X^{vs}$ is the normal vector to the virtual surface. This condition seems reasonable, considering that the virtual surface can be defined by both the solid and liquid phases. In our configuration, the free surface moves with velocity $\mathbf{U}_f$, (S.A.4), and the interface moves with solid velocity $\mathbf{V}$ (S.A.7).

To introduce the flux through the interface, Meng and Wang consider a zero momentum jump at the virtual surface that is calculated from the momentum equations of the 3-D system,

$$(\sigma_s + \sigma_{f_m})\mathbf{N}_X^{vs} = \rho_s\varphi(\mathbf{V} - \mathbf{U})\Big((\mathbf{V} - \mathbf{V}_m) \cdot \mathbf{N}_X^{vs}\Big). \tag{S.B.14}$$

Then $\mathfrak{J}$ is introduced as the flux of granular mass through the interface in terms of the solid velocity,

$$\mathfrak{J} = -\rho_s\varphi(\partial_t(b + h) + \mathbf{V} \cdot \mathbf{N}_X^{vs}). \tag{S.B.15}$$

But using previous condition (S.B.13) and the definition of $\mathbf{V}_m$, $\mathfrak{J}$ is equivalently defined as

$$\mathfrak{J} = \rho_f(1 - \varphi)(\partial_t(b + h) + \mathbf{U} \cdot \mathbf{N}_X^{vs}). \tag{S.B.16}$$

So $\mathfrak{J}$ can also be interpreted as the flux of the fluid mass through the virtual surface. Notice that (S.B.16) is equivalent to our definition of the fluid mass flux at the interface $\rho_f\mathcal{V}_f$ introduced in (S.A.8), for $h = h_m$. As detailed in equation (S.B.11), we can identify $\rho_f\mathcal{V}_f$ and $\mathfrak{J}$ up to a coefficient. Nevertheless, instead of (S.B.15) we have (S.A.7) and (S.A.8), where we establish that the fluid mass flux is exactly balanced by the upper fluid layer and that the solid phase does not leave the mixture layer. In the Meng-Wang model the flux $\mathfrak{J}$ describes both the solid entering the mixture and the fluid expelled or the contrary. By using again the kinematic condition (S.B.13) it is possible to write the following alternative expression

$$\mathfrak{J} = -\rho_s\varphi(\mathbf{V} - \mathbf{V}_m) \cdot \mathbf{N}_X^{vs}, \tag{S.B.17}$$

hence the momentum condition (S.B.14) is equivalently written as

$$(\sigma_s + \sigma_{f_m})\mathbf{N}_X^{vs} = -(\mathbf{V} - \mathbf{U})\,\mathfrak{J}. \tag{S.B.18}$$

Besides the different velocities, this condition looks similar to the total momentum conservation (S.A.9) where σ_f is neglected. As we discussed in section S.A.3 this quantity must be distributed among the phases in order to have complete boundary conditions. In Meng & Wang (2018) this distribution is made through the coefficient $\lambda = 1 - \varphi$ as follows

$$\begin{aligned} \sigma_s\mathbf{N}_X^{vs} &= -(1 - \lambda)(\mathbf{V} - \mathbf{U})\mathfrak{J}, \\ \sigma_{f_m}\mathbf{N}_X^{vs} &= -\lambda(\mathbf{V} - \mathbf{U})\mathfrak{J}. \end{aligned} \tag{S.B.19}$$

By denoting E_f^{MW} the corresponding tangential projection of the flux as in (S.A.10), $E_f^{\mathrm{MW}} =$

$(\mathbf{V}-\mathbf{U})_{\mathrm{tg}}\,\Im$, the tangent component of previous relations reads

$$(\sigma_s \mathbf{N}_X^{vs})_{\mathrm{tg}} = -(1-\lambda)E_f^{\mathrm{MW}},$$
$$(\sigma_{f_m} \mathbf{N}_X^{vs})_{\mathrm{tg}} = -\lambda E_f^{\mathrm{MW}}. \tag{S.B.20}$$

So they also follow the same form as in (S.A.12), where F_d (drag term) is neglected. Again, this highlights that, due to the virtual surface, the solid that enters the mixture replaces the equivalent mass of fluid in the mixture while the solid expelled from the mixture is replaced by the equivalent mass of fluid.

S.C. Additional material for simplified models

S.C.1. *Calculation details of the two-phase model (B1)*

The model (B1) presented in section 4 is based on the assumption that the upper-fluid layer moves with the mixture velocity $\mathbf{v}_m$ assuming $k_f \to \infty$ in the full model (A1). The final model reads as follows. The mass conservation equations are the same as in the original model:

$$\partial_t(\rho_s \varphi h_m) + \nabla\cdot(\rho_s \varphi h_m \mathbf{v}) = 0, \tag{S.C.1a}$$

$$\partial_t(\rho_f(1-\varphi)h_m) + \nabla\cdot(\rho_f(1-\varphi)h_m \mathbf{u}) = -\rho_f \mathcal{V}_f, \tag{S.C.1b}$$

$$\partial_t(\rho_f h_f) + \nabla\cdot(\rho_f h_f \mathbf{v}_m) = \rho_f \mathcal{V}_f, \tag{S.C.1c}$$

with the same expression of the fluid transfer rate

$$\mathcal{V}_f = -h_m\Phi - \nabla\cdot(h_m(1-\varphi)(\mathbf{u}-\mathbf{v})), \tag{S.C.2}$$

or alternatively the continuity equation for the solid volume fraction

$$\partial_t\varphi + \mathbf{v}\cdot\nabla\varphi = -\varphi\Phi. \tag{S.C.3}$$

The momentum equations read

$$\begin{aligned}
&\partial_t\left(\rho_s\varphi\left(h_m\mathbf{v} + \frac{\rho_f h_f}{\rho}\mathbf{v}_m\right)\right) + \nabla\cdot\left(\rho_s\varphi\left(h_m\mathbf{v}\otimes\mathbf{v} + \frac{\rho_f h_f}{\rho}\mathbf{v}_m\otimes\mathbf{v}_m\right)\right)\\
&= -g\cos\theta\nabla\left((\rho_s-\rho_f)\varphi\frac{h_m^2}{2} + \rho_f\frac{(h_m+h_f)^2}{2}\right) + g\cos\theta(\rho h_m + \rho_f h_f)\frac{\rho_f(1-\varphi)}{\rho}\nabla(h_m+h_f)\\
&\quad - (\rho h_m + \rho_f h_f)\frac{\rho_s\varphi}{\rho}g\cos\theta\nabla b + (1-\varphi)h_m\overline{\nabla p^e_{f_m}} + \beta h_m(\mathbf{u}-\mathbf{v})\\
&\quad - \mathrm{sgn}(\mathbf{v})\mu\left(\varphi(\rho_s-\rho_f)g\cos\theta h_m - (p^e_{f_m})_{|b}\right) + \frac{\rho_s\varphi}{\rho}((1-\lambda_f)\mathbf{u} + \lambda_f\mathbf{v}_m)\rho_f\mathcal{V}_f\\
&\quad - (\rho h_m + \rho_f h_f)\frac{\rho_s\varphi}{\rho}g\sin\theta\mathbf{e}_x - \frac{\rho_f^2\rho_s}{\rho^2}h_f\mathbf{v}_m(\varphi\Phi + (\mathbf{v}-\mathbf{v}_m)\cdot\nabla\varphi),
\end{aligned} \tag{S.C.4a}$$

$$
\begin{aligned}
&\partial_t\left(\rho_f(1-\varphi)\left(h_m\mathbf{u}+\frac{\rho_f h_f}{\rho}\mathbf{v}_m\right)\right)+\nabla\cdot\left(\rho_f(1-\varphi)\left(h_m\mathbf{u}\otimes\mathbf{u}+\frac{\rho_f h_f}{\rho}\mathbf{v}_m\otimes\mathbf{v}_m\right)\right)\\
&=-(\rho h_m+\rho_f h_f)\frac{\rho_f(1-\varphi)}{\rho}g\cos\theta\nabla(b+h_m+h_f)-(1-\varphi)h_m\overline{\nabla p^e_{f_m}}\\
&\quad-\beta h_m(\mathbf{u}-\mathbf{v})-\frac{\rho_s\varphi}{\rho}((1-\lambda_f)\mathbf{u}+\lambda_f\mathbf{v}_m)\rho_f\mathcal{V}_f-\frac{5}{2}\frac{\eta_e(1-\varphi)}{h_m}\mathbf{u}\\
&\quad-(\rho h_m+\rho_f h_f)\frac{\rho_f(1-\varphi)}{\rho}g\sin\theta\mathbf{e}_x+\frac{\rho_f^2\rho_s}{\rho^2}h_f\mathbf{v}_m(\varphi\Phi+(\mathbf{v}-\mathbf{v}_m)\cdot\nabla\varphi).
\end{aligned}
\tag{S.C.4b}
$$

The closures are again the original ones, given by equations (2.20)-(2.26).

The combination of momentum equations can not a priori be written in a conservative form and some calculations are needed to obtain the proposed equations (S.C.4). We detail such calculation for clarity.

The total momentum conservation equation, as the sum of equations in (2.18), reads

$$
\begin{aligned}
&\partial_t\left((\rho h_m+\rho_f h_f)\mathbf{v}_m\right)+\nabla\cdot\left(\rho_s\varphi h_m\mathbf{v}\otimes\mathbf{v}+\rho_f(1-\varphi)h_m\mathbf{u}\otimes\mathbf{u}+\rho_f h_f\mathbf{v}_m\otimes\mathbf{v}_m\right)\\
&=-g\cos\theta\nabla\left((\rho_s-\rho_f)\varphi\frac{h_m^2}{2}+\rho_f\frac{(h_m+h_f)^2}{2}\right)\\
&\quad-\operatorname{sgn}(\mathbf{v})\mu\left(\varphi(\rho_s-\rho_f)g\cos\theta h_m-(p^e_{f_m})_{|b}\right)\\
&\quad-\frac{5}{2}\frac{\eta_e(1-\varphi)}{h_m}\mathbf{u}-(\rho h_m+\rho_f h_f)(g\cos\theta\nabla b+g\sin\theta\mathbf{e}_x).
\end{aligned}
\tag{S.C.5}
$$

The combination of the fluid equations (2.18*b*) + $\frac{\rho_f(1-\varphi)}{\rho}\times$ (2.18*c*) gives

$$
\begin{aligned}
&\partial_t(\rho_f(1-\varphi)h_m\mathbf{u})+\nabla\cdot(\rho_f(1-\varphi)h_m\mathbf{u}\otimes\mathbf{u})+\frac{\rho_f(1-\varphi)}{\rho}\left(\partial_t(\rho_f h_f\mathbf{v}_m)+\nabla\cdot(\rho_f h_f\mathbf{v}_m\otimes\mathbf{v}_m)\right)\\
&=-(1-\varphi)\frac{\rho h_m+\rho_f h_f}{\rho}\rho_f g\cos\theta\nabla(b+h_m+h_f)-(1-\varphi)h_m\overline{\nabla p^e_{f_m}}-\beta h_m(\mathbf{u}-\mathbf{v})\\
&\quad-\frac{\rho_s\varphi}{\rho}((1-\lambda_f)\mathbf{u}+\lambda_f\mathbf{v}_m)\rho_f\mathcal{V}_f-\frac{5}{2}\frac{\eta_e(1-\varphi)}{h_m}\mathbf{u}-(1-\varphi)\frac{\rho h_m+\rho_f h_f}{\rho}\rho_f g\sin\theta\mathbf{e}_x.
\end{aligned}
\tag{S.C.6}
$$

We work on (S.C.6) to find a conservative formulation. Notice that

$$
\frac{\rho_f(1-\varphi)}{\rho}\partial_t(\rho_f h_f\mathbf{v}_m)=\partial_t\left(\frac{\rho_f(1-\varphi)}{\rho}\rho_f h_f\mathbf{v}_m\right)+\frac{\rho_f^2\rho_s}{\rho^2}h_f\mathbf{v}_m\partial_t\varphi
$$

and

$$
\frac{\rho_f(1-\varphi)}{\rho}\nabla\cdot(\rho_f h_f\mathbf{v}_m\otimes\mathbf{v}_m)=\nabla\cdot\left(\frac{\rho_f(1-\varphi)}{\rho}\rho_f h_f\mathbf{v}_m\otimes\mathbf{v}_m\right)+\frac{\rho_f^2\rho_s}{\rho^2}h_f(\mathbf{v}_m\otimes\mathbf{v}_m)\nabla\varphi
$$

where we used $\phi\nabla\cdot(\mathbf{w}_1\otimes\mathbf{w}_2)=\nabla\cdot(\phi\mathbf{w}_1\otimes\mathbf{w}_2)-(\mathbf{w}_1\otimes\mathbf{w}_2)^t\nabla\phi$ for any scalar ϕ and any vectors $\mathbf{w}_1,\mathbf{w}_2$.

Now we use (S.C.3) to write the two terms on φ, using also that $(\mathbf{w}_1\otimes\mathbf{w}_2)\nabla\phi=\mathbf{w}_1(\mathbf{w}_2\cdot\nabla\phi)$,

$$
\frac{\rho_f^2\rho_s}{\rho^2}h_f(\mathbf{v}_m\partial_t\varphi+(\mathbf{v}_m\otimes\mathbf{v}_m)\nabla\varphi)=\frac{\rho_f^2\rho_s}{\rho^2}h_f\mathbf{v}_m(-\varphi\Phi+(\mathbf{v}_m-\mathbf{v})\cdot\nabla\varphi).
$$

Hence (S.C.6) finally reads as in (S.C.4*b*)

$$\begin{aligned}
&\partial_t\left(\rho_f(1-\varphi)\left(h_m\mathbf{u}+\frac{\rho_f h_f}{\rho}\mathbf{v}_m\right)\right)+\nabla\cdot\left(\rho_f(1-\varphi)\left(h_m\mathbf{u}\otimes\mathbf{u}+\frac{\rho_f h_f}{\rho}\mathbf{v}_m\otimes\mathbf{v}_m\right)\right)\\
&=-(\rho h_m+\rho_f h_f)\frac{\rho_f(1-\varphi)}{\rho}g\cos\theta\nabla(b+h_m+h_f)-(1-\varphi)h_m\overline{\nabla p^e_{f_m}}\\
&\quad-\beta h_m(\mathbf{u}-\mathbf{v})-\frac{\rho_s\varphi}{\rho}((1-\lambda_f)\mathbf{v}_m+\lambda_f\mathbf{u})\rho_f\mathcal{V}_f-\frac{5}{2}\frac{\eta_e(1-\varphi)}{h_m}\mathbf{u}\\
&\quad-(\rho h_m+\rho_f h_f)\frac{\rho_f(1-\varphi)}{\rho}g\sin\theta\mathbf{e}_x+\frac{\rho_f^2\rho_s}{\rho^2}h_f\mathbf{v}_m(\varphi\Phi+(\mathbf{v}-\mathbf{v}_m)\cdot\nabla\varphi).
\end{aligned}\tag{S.C.7}$$

An alternative momentum equation is found by subtracting equation (S.C.7) from the total one (S.C.5), thus obtaining an equation involving the solid phase velocity (S.C.4*a*).

Notice that neither (S.C.6) nor (S.C.4*a*) are the conservation momentum equation for the solid and fluid phases because they have been obtained as a special combination of the original equations. These equations are written straightforward in terms of the virtual thickness H yielding (4.4*d*) and (4.4*e*).

Let us detail the writing of the solid mass equation (4.4*a*) in terms of H for the readers' convenience. Those for the fluid phase being equivalent. From the solid mass equation (S.C.1*a*) using the definition of H we write

$$\partial_t(\varphi H)+\nabla\cdot(\varphi H\mathbf{v})=\partial_t\left(\frac{\rho_f}{\rho}\varphi h_f\right)+\nabla\cdot\left(\frac{\rho_f}{\rho}\varphi h_f\mathbf{v}\right).$$

Now we use the equation of h_f to write

$$\partial_t\left(\frac{\rho_f}{\rho}\varphi h_f\right)=\frac{\rho_f}{\rho}\left(\varphi\mathcal{V}_f-\frac{\rho_f}{\rho}h_f\varphi\Phi-\varphi\nabla\cdot(h_f\mathbf{v}_m)-\frac{\rho_f}{\rho}h_f\mathbf{v}\cdot\nabla\varphi\right)$$

and we develop

$$\nabla\cdot\left(\frac{\rho_f}{\rho}\varphi h_f\mathbf{v}\right)=\frac{\rho_f}{\rho}h_f\mathbf{v}\cdot\nabla\varphi+\varphi\nabla\cdot\left(\frac{\rho_f}{\rho}h_f\mathbf{v}\right).$$

Using the expression of $\mathcal{V}_f$ in (S.C.2) and rearranging terms we find

$$\partial_t(\varphi H)+\nabla\cdot(\varphi H\mathbf{v})=-\frac{\rho_f}{\rho}\varphi H\Phi-\frac{\rho_f}{\rho}\varphi\nabla\cdot\left(h_m(1-\varphi)(\mathbf{u}-\mathbf{v})+h_f(\mathbf{v}_m-\mathbf{v})\right).$$

Notice that from the definition of the mixture velocity $\mathbf{v}_m$ we write $\mathbf{v}_m-\mathbf{v}=\frac{\rho_f(1-\varphi)(\mathbf{u}-\mathbf{v})}{\rho}$, then it yields (4.4*a*).

S.C.2. *Alternative simplified models*

In this section we present other simplified versions of the full model (A1) by considering different ideas. Namely we propose a one-layer one-velocity model where the solid mass is conserved instead of the total mass. Next two options already presented in previous works for two-layers two-velocities models are summarized. For the first one, originally presented in Drach (2023), the phases in the mixture are supposed to have the same velocity leading to the (A2) model (figure 3**A2**). The second one, presented in Bouchut et al. (2016), is obtained by considering that the fluid phases (in the mixture and in the upper layer) move with the same velocity (see figure S7).

S.C.2.1. *One-layer one-velocity model with solid mass conservation*

We present here an alternative one-velocity model to the oversimplified model (C2) presented in Section 3. The idea is to preserve the conservation of solid mass instead of total mass, and to use the acceleration equation instead of total momentum conservation. With this choice, we do not preserve the total mass or the fluid mass. The interpretation of such a system could be to consider a mixture layer of fluid and granular material with an 'infinite' fluid layer above, from which we can always expel some fluid when contraction occurs, and from where we can always absorb some fluid when dilation occurs. The dilatancy effect in the model is retained, as in model (3.13), appearing in the continuity equation of the volume fraction and as a part of the friction law through the excess pore pressure $p^e_{f_m}$.

As in section 3.2, we aim to find a model with a unique thickness and one velocity. In model (C2), we preserved the total mass conservation ρH with the objective of finding the Iverson-George model. However, as mentioned in Section 3.2, for that choice, neither the solid mass nor the fluid mass are preserved. In the model proposed here, we maintain h_m as the unique thickness of the model, and we neglect h_f in the system. Consequently, similar to model (C2), we do not solve equation (3.2*b*). The proposed alternative mixture model for unknowns $h_m, \varphi, \mathbf{v}$ is given by the following equations

$$\partial_t(\varphi h_m) + \nabla\cdot(\varphi h_m \mathbf{v}) = 0, \tag{S.C.8a}$$

$$\partial_t \varphi + \mathbf{v}\cdot\nabla\varphi = -\varphi\Phi, \tag{S.C.8b}$$

$$\begin{aligned}\partial_t(\rho h_m \mathbf{v}) + \nabla\cdot\Big(\rho h_m \mathbf{v}\otimes\mathbf{v}\Big) + g\cos\theta\nabla\Big(\rho\frac{h_m^2}{2}\Big) - \rho_f h_m \mathbf{v}\Phi \\ = -\rho h_m g\cos\theta\nabla b - \rho h_m g\sin\theta\mathbf{e}_x - \mathrm{sgn}(\mathbf{v})\mu\left((\rho-\rho_f)g\cos\theta h_m - (p^e_{f_m})_{|b}\right) - \frac{5}{2}\frac{\eta_e(1-\varphi)}{h_m}\mathbf{v},\end{aligned} \tag{S.C.8c}$$

together with relations in (2.22) and (2.20*b*) for the dilatancy law and the pore pressure. Notice that the term $\rho_f h_m \mathbf{v}\Phi$ in the momentum equation must be added to be consistent with the considered mass equations.

As we mentioned before, the model (S.C.8) conserve solid mass and volume, but it does not preserve the total mass and the fluid mass and neither their associated volumes. If we write them from (S.C.8) we find the following equations for the volumes,

$$\begin{aligned}\text{total volume:} \quad & \partial_t h_m + \nabla\cdot(h_m\mathbf{v}) = h_m\Phi, \\ \text{fluid volume:} \quad & \partial_t((1-\varphi)h_m) + \nabla\cdot((1-\varphi)h_m\mathbf{v}) = h_m\Phi,\end{aligned}$$

and for the masses

$$\begin{aligned}\text{total mass:} \quad & \partial_t(\rho h_m) + \nabla\cdot(\rho h_m\mathbf{v}) = \rho_f h_m\Phi, \\ \text{fluid mass:} \quad & \partial_t(\rho_f(1-\varphi)h_m) + \nabla\cdot(\rho_f(1-\varphi)h_m\mathbf{v}) = \rho_f h_m\Phi.\end{aligned} \tag{S.C.9}$$

As for the model (C2), these equations show that the conservation of volume and mass are recovered at the order of the dilatancy Φ (supposed to be small in this case).

S.C.2.2. *Two layer model with one velocity in the mixture and one velocity in the upper-fluid layer (A2)*

This model, presented in Drach (2023), is obtained as the limit of the complete model when the friction coefficient between the two phases in the mixture β tends to infinity, that leads $\mathbf{u} = \mathbf{v}$ as we did to obtain the model (C1). We thus consider that the fluid and solid phases in the mixture moves with the same velocity, that also equals the velocity of the mixture $\mathbf{v}_m = \mathbf{v}$.

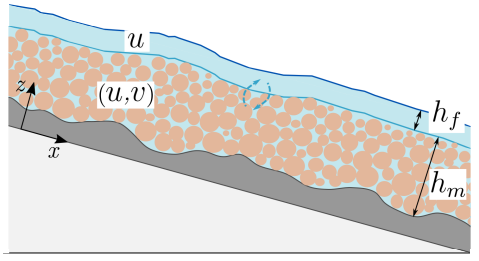

Figure S7: Sketch for the two-layer model with two velocities in the mixture and the upper-fluid velocity $\mathbf{u}$.

Nevertheless we keep a different velocity for the fluid upper layer, $\mathbf{u}_f$ (see figure 3**A2**). We write the obtained model for unknowns $h_m, h_f, \varphi, \mathbf{v}, \mathbf{u}_f$. The mass equations read

$$\partial_t h_m + \nabla \cdot (h_m \mathbf{v}) = -\mathcal{V}_f, \tag{S.C.10a}$$

$$\partial_t h_f + \nabla \cdot (h_f \mathbf{u}_f) = \mathcal{V}_f, \tag{S.C.10b}$$

$$\partial_t \varphi + \mathbf{v} \cdot \nabla \varphi = -\varphi \Phi. \tag{S.C.10c}$$

The momentum conservation equation for the mixture is the sum of (2.18*a*) and (2.18*b*),

$$\begin{aligned}\partial_t(\rho h_m \mathbf{v}) + \nabla \cdot (\rho h_m \mathbf{v} \otimes \mathbf{v}) = &-\rho h_m g \cos\theta \nabla(b + h_m) - \rho_f h_m g \cos\theta \nabla h_f \\ &-(\rho_s - \rho_f) g \cos\theta \frac{h_m^2}{2} \nabla \varphi - ((1-\lambda_f)\mathbf{v} + \lambda_f \mathbf{u}_f)\rho_f \mathcal{V}_f \\ &- \operatorname{sgn}(\mathbf{v}) \mu \left(\varphi(\rho_s - \rho_f) g \cos\theta h_m - (p^e_{f_m})_{|b} \right) \\ &+ k_f(\mathbf{u}_f - \mathbf{v}) - \frac{5}{2} \frac{\eta_e (1-\varphi)}{h_m} \mathbf{v} - \rho h_m g \sin\theta \mathbf{e}_x .\end{aligned} \tag{S.C.11a}$$

Finally the momentum equation for the upper fluid layer does not change and it is given by (2.18*c*),

$$\begin{aligned}\partial_t(\rho_f h_f \mathbf{u}_f) + \nabla \cdot (\rho_f h_f \mathbf{u}_f \otimes \mathbf{u}_f) = &-\rho_f h_f g \cos\theta \nabla(b + h_m + h_f) \\ &+((1-\lambda_f)\mathbf{v} + \lambda_f \mathbf{u}_f)\rho_f \mathcal{V}_f - k_f(\mathbf{u}_f - \mathbf{v}) \\ &-\rho_f h_f g \sin\theta \mathbf{e}_x .\end{aligned} \tag{S.C.11b}$$

The fluid transfer rate in (2.25) gives $\mathcal{V}_f = -h_m \Phi$. Notice that the excess pore pressure only appear in the friction term at the bottom. The closures are the same as for the original model in (2.20*b*)-(2.26).

S.C.2.3. *Two-layer model with one velocity for each phase*

This simplification was already presented in Section 4.3 of Bouchut et al. (2016), but we include it here for the sake of completeness for our hierarchy of models. Remember that in Bouchut et al. (2016) the friction between the layers at the interface was taken proportional to $(\mathbf{u}_f - \mathbf{u})$. This model was thus obtained as the limit of an infinity friction between the layers, that leads to equal velocity of the fluid phase in the mixture and in the upper-fluid layer $\mathbf{u}_f = \mathbf{u}$ (see figure S7).

The resulting model with unknowns $h_m, h_f, \varphi, \mathbf{u}, \mathbf{v}$ states as follows. The mass equations read

$$\partial_t(\varphi h_m) + \nabla \cdot (\varphi h_m \mathbf{v}) = 0, \tag{S.C.12a}$$

$$\partial_t((1-\varphi)h_m + h_f) + \nabla\cdot(((1-\varphi)h_m + h_f)\mathbf{u}) = 0, \tag{S.C.12b}$$

$$\partial_t\varphi + \mathbf{v}\cdot\nabla\varphi = -\varphi\Phi. \tag{S.C.12c}$$

The momentum conservation equations are

$$\begin{aligned}\partial_t(\rho_s\varphi h_m\mathbf{v}) + \nabla\cdot(\rho_s\varphi h_m\mathbf{v}\otimes\mathbf{v}) = &-\varphi h_m g\cos\theta(\rho_s\nabla(b+h_m) + \rho_f\nabla h_f)\\ &-(\rho_s-\rho_f)g\cos\theta\frac{h_m^2}{2}\nabla\varphi + (1-\varphi)h_m\overline{\nabla p^e_{f_m}}\\ &-\operatorname{sgn}(\mathbf{v})\mu\left(\varphi(\rho_s-\rho_f)g\cos\theta h_m - (p^e_{f_m})_{|b}\right)\\ &+\beta h_m(\mathbf{u}-\mathbf{v}) - \varphi h_m\rho_s g\sin\theta\mathbf{e}_x,\end{aligned} \tag{S.C.12d}$$

$$\begin{aligned}\partial_t(\rho_f((1-\varphi)h_m + h_f)\mathbf{u}) + \nabla\cdot(\rho_f((1-\varphi)h_m + h_f)\mathbf{u}\otimes\mathbf{u})&\\ = -((1-\varphi)h_m + h_f)\rho_f g\cos\theta\nabla(b+h_m+h_f)&\\ -(1-\varphi)h_m\overline{\nabla p^e_{f_m}} - \frac{5}{2}\frac{\eta_e(1-\varphi)}{h_m}\mathbf{u}&\\ -\beta h_m(\mathbf{u}-\mathbf{v}) - ((1-\varphi)h_m + h_f)\rho_f g\sin\theta\mathbf{e}_x.&\end{aligned} \tag{S.C.12e}$$

Notice that the exchange term no longer appears in this two-velocity model. The closures are the same as for the original model, given by equations (2.20*a*)-(2.24). The energy balance of this model has been already presented in Bouchut et al. (2016).

S.D. Additional material for numerical test

S.D.1. *Models in uniform regime*

In this section a summary of the models in uniform 1-D configuration is presented. The bold format is then removed for velocities notation, that now read v, u, u_f, v_m. First we present our series of models, accordingly to the classification made in figure 3, then we write the Iverson-George model and the Meng-Wang model.

S.D.1.1. *Our hierarchy of models in uniform regime*

(A1) Two-layer model with three velocities

The complete model (2.16)-(2.25) for unknowns $h_m, h_f, \varphi, v, u, u_f$ in uniform regime, taking into account that $\mathcal{V}_f = -h_m\Phi$, reads as follows.

$$\partial_t h_m = h_m\Phi, \tag{S.D.1a}$$

$$\partial_t h_f = -h_m\Phi, \tag{S.D.1b}$$

$$\partial_t\varphi = -\varphi\Phi, \tag{S.D.1c}$$

$$\partial_t v = -\mu\operatorname{sgn}(v)\frac{p_{s\,|b}}{\rho_s\varphi h_m} + \frac{\beta}{\rho_s\varphi}(u-v) + \frac{k_f}{\rho h_m}(u_f - v_m) - g\sin\theta\mathbf{e}_x, \tag{S.D.1d}$$

$$\partial_t u = -\lambda_f\frac{\Phi}{(1-\varphi)}(u-u_f) - \frac{\beta}{\rho_f(1-\varphi)}(u-v) + \frac{k_f}{\rho h_m}(u_f-v_m) - \frac{5}{2}\frac{\eta_e}{\rho_f h_m^2}u - g\sin\theta\mathbf{e}_x, \tag{S.D.1e}$$

$$\partial_t u_f = -(1-\lambda_f)\frac{h_m\Phi}{h_f}(u-u_f) - \frac{k_f}{\rho_f h_f}(u_f - v_m) - g\sin\theta\mathbf{e}_x, \tag{S.D.1f}$$

together with the following closures

$$\beta = \frac{150\eta_f\varphi^2}{(1-\varphi)d^2}, \quad k_f = \frac{\rho h_m \rho_f h_f}{\rho h_m + \rho_f h_f}|u_f - v_m|, \quad \lambda_f = \frac{1}{2} + \frac{1}{2}\,\mathrm{sgn}(\Phi)\delta_f, \quad \delta_f = \begin{cases} 0 & \text{centered dist.,} \\ 1 & \text{upwind dist.,} \end{cases} \tag{S.D.2a}$$

and the effective viscosity $\eta_e = \eta_f(1 + \frac{5}{2}\varphi)$. The friction coefficient is

$$\mu = (\mu^{\mathrm{eq}} + K(\varphi - \varphi^{\mathrm{eq}}))_+ . \tag{S.D.2b}$$

The rheological laws give

$$\begin{aligned} &\varphi^{\mathrm{eq}} = \frac{\varphi_c}{1 + b_\varphi \mathcal{J}_\varphi^{1/2}} \quad \text{with} \quad \mathcal{J}_\varphi = \alpha_\varphi I^2 + J, \\ &\mu^{\mathrm{eq}} = \mu_c + \frac{\Delta\mu}{1 + I_0/\mathcal{J}_\mu^{1/2}} \quad \text{with} \quad \mathcal{J}_\mu = \alpha_\mu I^2 + J, \\ &\text{where} \quad I = \frac{d\,\dot\gamma}{\sqrt{p_{s|b}/\rho_s}}, \quad J = \frac{\eta_f \dot\gamma}{p_{s|b}}, \quad \dot\gamma = \frac{5}{2}\frac{|v|}{h_m}. \end{aligned} \tag{S.D.2c}$$

As we discussed previously, there are two options to set the definition of the basal solid pressure.

Option 1 for the computation of $p_{s|b}$. The first option is done by the definition of the basal solid pressure $p_{s|b}$ as $p_{s|b} = \varphi(\rho_s - \rho_f)g\cos\theta h_m - (p^e_{f_m})_{|b}$, with $(p^e_{f_m})_{|b} = -\frac{\beta}{(1-\varphi)^2}\frac{h_m^2}{2}\Phi$, where the dilatancy function (S.D.1) is given by

$$\Phi = \dot\gamma K(\varphi - \varphi^{\mathrm{eq}}). \tag{S.D.3a}$$

Note that taking into account the definition of φ^{eq}, it implies an implicit definition of $p_{s|b}$. Namely, as explained in Section 2.3.2, it can be seen that $\sqrt{p_{s|b}}$ is a root of a third order polynomial,

$$\begin{aligned} &(\sqrt{p_{s|b}})^3 + A_2(\sqrt{p_{s|b}})^2 \\ &-(\varphi(\rho_s - \rho_f)g\cos\theta h_m + A_1(\varphi - \varphi_c))(\sqrt{p_{s|b}}) - A_2(\varphi(\rho_s - \rho_f)g\cos\theta h_m + \varphi A_1) = 0 \end{aligned} \tag{S.D.3b}$$

with coefficients $A_1 = \dfrac{\beta}{(1-\varphi)^2}\dfrac{h_m^2}{2}\dot\gamma K$, $A_2 = b\,(\alpha_\varphi d^2\dot\gamma^2\rho_s + \eta_f\dot\gamma)^{1/2}$.

Option 2 for the computation of $p_{s|b}$ The basal solid pressure is the solution of the following equation

$$\partial_t p_{s|b} = -\frac{3}{2}B(\Phi - \dot\gamma K(\varphi - \varphi^{\mathrm{eq}})), \tag{S.D.4a}$$

with B the solid bulk modulus. In this case, the dilatancy function Φ is written in terms of the basal solid pressure using the expression of $(p^e_{f_m})_{|b}$ that gives

$$\Phi = \frac{2(1-\varphi)^2}{\beta h_m^2}(p_{s|b} - \varphi(\rho_s - \rho_f)g\cos\theta h_m). \tag{S.D.4b}$$

(A2) Two-layer model with one velocity in the mixture and an independent velocity in the upper-layer

The model with two velocities and an upper fluid layer in section S.C.2.2, with unknowns $h_m, h_f, \varphi, u_f, v$ given in (S.C.10)-(S.C.11) reads

$$\partial_t h_m = h_m \Phi, \tag{S.D.5a}$$

$$\partial_t h_f = -h_m \Phi, \tag{S.D.5b}$$

$$\partial_t \varphi = -\varphi \Phi, \tag{S.D.5c}$$

$$\partial_t v = \frac{\rho_f}{\rho}\lambda_f \Phi(u_f - v) - \mu\,\mathrm{sgn}(v)\frac{p_{s|b}}{\rho h_m} + \frac{k_f}{\rho h_m}(u_f - v) - \frac{5}{2}\frac{\eta_e(1-\varphi)}{\rho h_m^2}v - g\sin\theta \mathbf{e}_x, \tag{S.D.5d}$$

$$\partial_t u_f = (1-\lambda_f)\frac{h_m \Phi}{h_f}(u_f - v) - \frac{k_f}{\rho_f h_f}(u_f - v) - g\sin\theta \mathbf{e}_x, \tag{S.D.5e}$$

together with the following closures

$$\lambda_f = \frac{1}{2} + \frac{1}{2}\,\mathrm{sgn}(\Phi)\delta_f, \quad \delta_f = \begin{cases} 0 & \text{centered distribution,} \\ 1 & \text{upwind distribution,} \end{cases} \tag{S.D.6a}$$

$k_f = \frac{\rho h_m \rho_f h_f}{\rho h_m + \rho_f h_f}|u_f - v|$ and $\eta_e = \eta_f(1 + \frac{5}{2}\varphi)$. The friction coefficient is

$$\mu = (\mu^{\mathrm{eq}} + K(\varphi - \varphi^{\mathrm{eq}}))_+ . \tag{S.D.6b}$$

The rheological laws are

$$\begin{aligned} &\varphi^{\mathrm{eq}} = \frac{\varphi_c}{1 + b_\varphi \mathcal{J}_\varphi^{1/2}} \quad \text{with} \quad \mathcal{J}_\varphi = \alpha_\varphi I^2 + J, \\ &\mu^{\mathrm{eq}} = \mu_c + \frac{\Delta\mu}{1 + I_0/\mathcal{J}_\mu^{1/2}} \quad \text{with} \quad \mathcal{J}_\mu = \alpha_\mu I^2 + J, \\ &\text{where} \quad I = \frac{d\,\dot\gamma}{\sqrt{p_{s|b}/\rho_s}}, \quad J = \frac{\eta_f \dot\gamma}{p_{s|b}}, \quad \dot\gamma = \frac{5}{2}\frac{|v|}{h_m}. \end{aligned} \tag{S.D.6c}$$

The basal solid pressure $p_{s|b}$ is defined as $p_{s|b} = \varphi(\rho_s - \rho_f)g\cos\theta h_m - (p^e_{f_m})_{|b}$, with $(p^e_{f_m})_{|b} = -\frac{\beta}{(1-\varphi)^2}\frac{h_m^2}{2}\Phi$. We also consider two possible computation.

Option 1. The basal solid pressure is calculated as the solution of the polynomial

$$(\sqrt{p_{s|b}})^3 + A_2(\sqrt{p_{s|b}})^2 - \Big(\varphi(\rho_s - \rho_f)g\cos\theta h_m + A_1(\varphi - \varphi_c)\Big)\sqrt{p_{s|b}} - A_2(\varphi(\rho_s - \rho_f)g\cos\theta h_m + A_1\varphi) = 0 \tag{S.D.7a}$$

with coefficients $A_1 = \dfrac{\beta}{(1-\varphi)^2}\dfrac{h_m^2}{2}\dot\gamma K$, $A_2 = a(\alpha_\varphi d^2\dot\gamma^2\rho_s + \eta_f\dot\gamma)$. The dilatancy function in equations (S.D.1) is given by

$$\Phi = \dot\gamma K(\varphi - \varphi^{\mathrm{eq}}). \tag{S.D.7b}$$

Option 2. The basal solid pressure is the solution of the following equation,

$$\partial_t p_{s|b} = -\frac{3}{2}B(\Phi - \dot\gamma K(\varphi - \varphi^{\mathrm{eq}})), \tag{S.D.8a}$$

with B the solid bulk modulus. The dilatancy function Φ is written in terms of the basal solid pressure using the expression of $(p^e_{f_m})_{|b}$ that gives

$$\Phi = \frac{2(1-\varphi)^2}{\beta h_m^2}(p_{s|b} - \varphi(\rho_s - \rho_f)g\cos\theta h_m). \tag{S.D.8b}$$

(B1) Two-layer model with two velocities in the mixture

The model with two velocities and an upper fluid layer with unknowns h_m, h_f, φ, u, v given in (S.C.1)-(S.C.4) reads

$$\partial_t h_m = h_m \Phi, \tag{S.D.9a}$$

$$\partial_t h_f = -h_m \Phi, \tag{S.D.9b}$$

$$\partial_t \varphi = -\varphi \Phi, \tag{S.D.9c}$$

$$\begin{aligned}\partial_t (h_m v + \frac{\rho_f}{\rho} h_f v_m) = &-\mu \operatorname{sgn}(v) \frac{p_{s|b}}{\rho_s \varphi} + \frac{\beta}{\rho_s \varphi} h_m (u - v) - (h_m + \frac{\rho_f}{\rho} h_f) g \sin\theta \mathbf{e}_x \\ &- \frac{\rho_f}{\rho}((1-\lambda_f)u + \lambda_f v_m) h_m \Phi + \left(h_m v + (1 - \frac{\rho_f}{\rho}) \frac{\rho_f}{\rho} h_f v_m \right) \Phi,\end{aligned} \tag{S.D.9d}$$

$$\begin{aligned}\partial_t (h_m u + \frac{\rho_f}{\rho} h_f v_m) = &-\frac{5}{2} \frac{\eta_e}{\rho_f h_m} u - \frac{\beta}{\rho_f (1-\varphi)} h_m (u - v) - (h_m + \frac{\rho_f}{\rho} h_f) g \sin\theta \mathbf{e}_x \\ &+ \frac{\rho_s \varphi}{\rho (1-\varphi)}((1-\lambda_f)u + \lambda_f v_m) h_m \Phi - \left(h_m u + (1 - \frac{\rho_f}{\rho}) \frac{\rho_f}{\rho} h_f v_m \right) \frac{\varphi}{1-\varphi} \Phi.\end{aligned} \tag{S.D.9e}$$

Closures for β, $p_{s|b}$ and Φ are the same given above in (S.D.2) and (S.D.3) or (S.D.4). Denoting $Q_v = h_m v + \frac{\rho_f}{\rho} h_f v_m$ and $Q_u = h_m u + \frac{\rho_f}{\rho} h_f v_m$, the primitive phases velocities u, v are recovered as follows

$$v = \frac{h_m Q_v + \frac{\rho_f^2}{\rho^2} h_f (Q_v - Q_u)}{h_m (h_m + \frac{\rho_f}{\rho} h_f)}, \quad u = \frac{Q_u - m v}{h_m + \frac{\rho_f^2}{\rho^2} h_f},$$

with $m = \frac{\rho_f \rho_s \varphi}{\rho^2} h_f$.

(B2) Two-layer model with one velocity

The model with an upper fluid layer (3.2) or equivalently (3.8)-(3.9) for unknowns h_m, h_f, φ, v reads

$$\partial_t h_m = h_m \Phi, \tag{S.D.10a}$$

$$\partial_t h_f = -h_m \Phi, \tag{S.D.10b}$$

$$\partial_t \varphi = -\varphi \Phi, \tag{S.D.10c}$$

$$\partial_t v = -\mu \operatorname{sgn}(v) \frac{p_{s|b}}{\rho h_m + \rho_f h_f} - \frac{5}{2} \frac{\eta_e (1-\varphi)}{(\rho h_m + \rho_f h_f) h_m} v - g \sin\theta \mathbf{e}_x. \tag{S.D.10d}$$

Closures for $p_{s|b}$ and Φ are the same given above in (S.D.2) and (S.D.3) or (S.D.4).

(C1) One-layer model with two velocities

The two-velocity model with one layer with unknowns H, φ, u, v given in (4.7) becomes

$$\partial_t H = \frac{\varphi(\rho_s - \rho_f)}{\rho} H \Phi^*, \tag{S.D.11a}$$

$$\partial_t \varphi = -\varphi \Phi^*, \tag{S.D.11b}$$

$$\partial_t v = -\mu \operatorname{sgn}(v) \frac{p_{s|b}^*}{\rho_s \varphi H} + \frac{\beta}{\rho_s \varphi}(u - v) - \frac{\rho_f}{\rho}((1-\lambda_f^*)u + \lambda_f^* v_m - v)\Phi^* - g \sin\theta \mathbf{e}_x, \tag{S.D.11c}$$

$$\partial_t u = -\frac{5}{2} \frac{\eta_e}{\rho_f H^2} u - \frac{\beta}{\rho_f (1-\varphi)}(u - v) + \frac{\rho_s \varphi}{\rho (1-\varphi)}((1-\lambda_f^*)u + \lambda_f^* v_m - u)\Phi^* - g \sin\theta \mathbf{e}_x. \tag{S.D.11d}$$

Closures for $\beta, \mu, p_{s|b}^*, \Phi^*$ are given in (S.D.13) and (S.D.14) or (S.D.15). The coefficient λ_f^* is defined analogously as

$$\lambda_f^* = \frac{1}{2} + \frac{1}{2}\,\mathrm{sgn}(\Phi^*)\delta_f, \quad \delta_f = \begin{cases} 0 & \text{centered distribution,} \\ 1 & \text{upwind distribution.} \end{cases}$$

(C2) One-layer model with one velocity

The model with 1 layer (3.13)-(3.14) with unknowns H, φ, v becomes

$$\partial_t H = \frac{\varphi(\rho_s - \rho_f)}{\rho} H\Phi^*, \tag{S.D.12a}$$

$$\partial_t \varphi = -\varphi\Phi^*, \tag{S.D.12b}$$

$$\partial_t v = -\mu^*\,\mathrm{sgn}(v)\frac{p_{s|b}^*}{\rho H} - \frac{5}{2}\frac{\eta_e(1-\varphi)}{\rho H^2} v - g\sin\theta \mathbf{e}_x. \tag{S.D.12c}$$

The closures in this case are analogous to (S.D.2) and they read as follows. The friction coefficient is

$$\mu^* = \left(\mu^{\mathrm{eq}*} + K(\varphi - \varphi^{\mathrm{eq}*})\right)_+. \tag{S.D.13a}$$

The rheological laws are

$$\begin{aligned} &\varphi^{\mathrm{eq}*} = \frac{\varphi_c}{1 + b_\varphi (\mathcal{J}_\varphi^*)^{1/2}} \quad \text{with} \quad \mathcal{J}_\varphi^* = \alpha_\varphi (I^*)^2 + J^*, \\ &\mu^{\mathrm{eq}*} = \mu_c + \frac{\Delta\mu}{I_0 + (\mathcal{J}_\mu^*)^{1/2}} (\mathcal{J}_\mu^*)^{1/2} \quad \text{with} \quad \mathcal{J}_\mu^* = \alpha_\mu (I^*)^2 + J^*, \\ &\text{where} \quad I^* = \frac{d\,\dot\gamma^*}{\sqrt{p_{s|b}^*/\rho_s}}, \quad J^* = \frac{\eta_f \dot\gamma^*}{p_{s|b}^*}, \quad \dot\gamma^* = \frac{5}{2}\frac{|v|}{H}. \end{aligned} \tag{S.D.13b}$$

We also have in this case two option to compute the basal solid pressure, denoted by $p_{s|b}^*$.

Option 1 for the computation of $p_{s|b}^*$. For this first option $p_{s|b}^*$ is defined by $p_{s|b}^* = \varphi(\rho_s - \rho_f) g\cos\theta H - (p_{f_m}^e)_{|b}^*$, with $(p_{f_m}^e)_{|b}^* = -\frac{\beta}{(1-\varphi)^2}\frac{h_m^2}{2}\Phi^*$, what implies again an implicit definition. The basal solid pressure is calculated as the root of a third order polynomial,

$$(\sqrt{p_{s|b}^*})^3 + A_2(\sqrt{p_{s|b}^*})^2 - \Big(\varphi(\rho_s - \rho_f) g\cos\theta H + A_1(\varphi - \varphi_c)\Big)\sqrt{p_{s|b}^*} - A_2(\varphi(\rho_s - \rho_f) g\cos\theta H + \varphi A_1) = 0 \tag{S.D.14a}$$

with coefficients $A_1 = \dfrac{\beta}{(1-\varphi)^2}\dfrac{h_m^2}{2}\dot\gamma^* K$, $A_2 = b(\alpha_\varphi d^2 (\dot\gamma^*)^2 \rho_s + \eta_f \dot\gamma^*)^{1/2}$. The dilatancy function is given by

$$\Phi^* = \dot\gamma^* K(\varphi - \varphi^{\mathrm{eq}*}). \tag{S.D.14b}$$

Option 2 for the computation of $p_{s|b}^*$. The basal solid pressure is the solution of the following equation,

$$\partial_t p_{s|b}^* = -\frac{3}{2} B(\Phi^* - \dot\gamma^* K(\varphi - \varphi^{\mathrm{eq}*})), \tag{S.D.15a}$$

with B the solid bulk modulus. The dilatancy function Φ^* is

$$\Phi^* = \frac{2(1-\varphi)^2}{\beta H^2}(p_{s|b}^* - \varphi(\rho_s - \rho_f) g\cos\theta H). \tag{S.D.15b}$$

S.D.1.2. *Other models in uniform regime*

Iverson-George model **[IG]**

Finally we write the Iverson-George model given in equations (3.17) in the uniform regime with unknowns h, φ, v, p_b.

$$\partial_t h = \frac{\varphi(\rho_s - \rho_f)}{\rho} D, \tag{S.D.16a}$$

$$\partial_t \varphi = -\varphi \frac{D}{h}, \tag{S.D.16b}$$

$$\partial_t v = -\frac{\tau_s + \tau_f}{\rho h} - g \sin\theta \mathbf{e}_x. \tag{S.D.16c}$$

$$\partial_t p_b = \frac{1}{4} g \cos\theta \rho_f \frac{\rho - \rho_f}{\rho} D + \frac{3}{2\alpha}\left(\frac{D}{h} - \dot{\gamma}_{\mathrm{IG}} \tan\psi_{\mathrm{IG}}\right). \tag{S.D.16d}$$

The closures are given as in (3.18*a*)-(3.18*e*) that read

$$\tau_f = (1-\varphi)\eta_e \frac{2v}{h}, \qquad \tau_s = \mu_{\mathrm{IG}} \frac{v}{|v|} \sigma_e, \qquad \mu_{\mathrm{IG}} = \tan(\delta + \psi_{\mathrm{IG}}), \tag{S.D.17a}$$

$$\sigma_e = \rho g \cos\theta h - p_b, \qquad p_b = \rho_f g \cos\theta h + p_e. \tag{S.D.17b}$$

The dilatancy function is

$$D = -\frac{2k_{\mathrm{IG}}}{h\eta_e} p_e, \qquad k_{\mathrm{IG}} = k_0 e^{\frac{0.6-\varphi}{0.04}}, \tag{S.D.17c}$$

and finally the rheological relations are

$$\tan\psi_{\mathrm{IG}} = \varphi - \varphi^{\mathrm{eq}}_{\mathrm{IG}}, \qquad \varphi^{\mathrm{eq}}_{\mathrm{IG}} = \frac{\varphi_c}{1 + \sqrt{N}}, \qquad N = \frac{J}{1 + I^2}, \qquad \dot{\gamma}_{\mathrm{IG}} = \frac{2|v|}{h}. \tag{S.D.17d}$$

Meng-Wang model **[MW]**

Lastly, we write the Meng-Wang model with unknowns h, φ, u, v given in (4.11) in the uniform regime. We use that

$$\mathfrak{J} = -\varphi \frac{\rho_f \rho_s}{\rho} h \Phi_{\mathrm{MW}}.$$

So it reads

$$\partial_t h = \frac{\varphi(\rho_s - \rho_f)}{\rho} h \Phi_{\mathrm{MW}}, \tag{S.D.18a}$$

$$\partial_t \varphi = -\varphi \Phi_{\mathrm{MW}}, \tag{S.D.18b}$$

$$\partial_t v = -\operatorname{sgn}(v)\mu_{\mathrm{MW}} \frac{p_{s\,|b}}{\rho_s \varphi h} + \frac{\beta_{\mathrm{MW}}}{\rho_s \varphi}(u - v) - g \sin\theta \mathbf{e}_x - (1-\lambda)(u-v)\frac{\rho_f}{\rho}\Phi_{\mathrm{MW}} - \frac{\alpha_s}{\rho_s h} v, \tag{S.D.18c}$$

$$\partial_t u = -\frac{\alpha_f}{\rho_f h} u - \frac{\beta_{\mathrm{MW}}}{\rho_f (1-\varphi)}(u - v) - g \sin\theta \mathbf{e}_x - \lambda(u - v)\frac{\varphi \rho_s}{\rho(1-\varphi)}\Phi_{\mathrm{MW}}. \tag{S.D.18d}$$

The closures are given in (4.11*f*)-(4.11*j*) and read

$$\Phi_{\mathrm{MW}} = \dot{\gamma}_{\mathrm{MW}} \tan\psi_{\mathrm{MW}}, \quad \tan\psi_{\mathrm{MW}} = K_1(\varphi - \varphi^{\mathrm{eq}}_{\mathrm{MW}}), \quad \varphi^{\mathrm{eq}}_{\mathrm{MW}} = \varphi_c - K_2 \frac{\eta_f \dot{\gamma}_{\mathrm{MW}}}{p_{s\,|b}},$$
$$\dot{\gamma}_{\mathrm{MW}} = 3\frac{|v|}{h}, \quad \mu_{\mathrm{MW}} = \tan(\delta + \psi_{\mathrm{MW}}), \qquad \beta_{\mathrm{MW}} = (1-\varphi)^2 \frac{\eta_f}{k_{\mathrm{MW}}}. \tag{S.D.19a}$$

The pressure terms are

$$p_{s|b} = \varphi(\rho_s - \rho_f)g\cos\theta h - (p_e)_{|b}, \qquad (p_e)_{|b} = -\frac{1}{2}\frac{\beta_{\mathrm{MW}}}{(1-\varphi)^2}h^2\Phi_{\mathrm{MW}}. \qquad \text{(S.D.19}b\text{)}$$

The distribution coefficient is $\lambda = 1-\varphi$, and the hydraulic permeability k_{MW}, and coefficients α_s, α_f are considered as constants.

S.D.2. *Test 1: Flow behavior in loose and dense cases*

In figure 5, we show the solid velocity v, the excess pore fluid pressure $(p^e_{fm})_{|b}$, solid volume fraction φ, friction coefficient μ and tangent of the dilatancy angle $\tan(\psi)$ for the loose and dense cases for both high and low viscosity. Let us first present the flow behavior obtained with the rheology proposed here that involves the dimensionless inertial and viscous numbers I^2 and J. Note that in the simulated cases I^2 is negligible for high viscosity and is only about 10% of J for low viscosity (see figure S10 of section S.D.3).

In the dense case, for both viscosities, the granular mass takes some time to start moving and then accelerates until it reaches the steady critical state (figure 5a,b). Since the beginning, the granular mass dilates (φ decreases and $\tan\psi > 0$) until it reaches the critical state (figure 5e,g). The excess pore pressure becomes negative during this transient regime (figure 5c,d) thus increasing the basal solid pressure (figure S11a,b). The positive dilatancy angle contributes to increase the effective friction coefficient μ at the beginning of the flow (figure 5g,h). These two effects contribute to increase the basal frictional shear stress, explaining why the mass takes time to start at the initial instants. Interestingly, since $\tan(\psi)$ decreases with time, dilatancy generates a friction weakening effect at the beginning of the flow that would not arise otherwise. Indeed, once $\tan(\psi)$ becomes very small after about 300 s for high viscosity and 20 s for low velocity, the friction coefficient increases, approaching to μ^{eq}, the evolution of which is dictated by the viscous-inertial number (figure 5g,h). Interestingly, the overall evolution of μ and $(p^e_{fm})_{|b}$ look very similar. This is partly related to the fact that $\dot\gamma$ is very small at the beginning (figure S11c,d) and thus the evolution of the two quantities follow the evolution of $\tan\psi$, while later on, $\dot\gamma$ increases and $\tan\psi$ becomes small so that $\dot\gamma$ controls their evolution as shown by the expression of μ and $(p^e_{fm})_{|b}$ in (2.4.3).

In the loose case, the mass starts to move at the beginning for the two viscosities. Let us first look at the behavior at high viscosity (dashed gray lines in the left column of figure 5). In that case, the mass acceleration is huge at the very beginning and then the velocity decreases until it reaches the steady critical state. Since the beginning, the granular mass compresses (φ increases and $\tan\psi < 0$) until it reaches the critical state. The excess pore pressure becomes positive during this transient regime thus significantly reducing the basal solid pressure p_{sb} (figure S11a,b) and therefore the basal frictional shear stress. This explain the higher velocity in the loose case compared to the dense case, despite the higher friction coefficient. Contrary to the dense case, φ approaches φ^{eq} at the very beginning since the negative dilatancy angle is very small, with a negligible contribution to the decrease of the effective friction coefficient μ (figure 5g). As a result μ is always very close to μ^{eq}. The friction coefficient is high at the beginning because of the high viscous-inertial number related to the high shear strain rate $\dot\gamma$ (figure S11c,d).

At first glance, it seems surprising that the behavior in the loose case is so different at low viscosity where the variables behave as in the dense case: increase of solid velocity, decrease of solid volume fraction and negative excess pore fluid pressure. In fact, the initial compaction in the so-called loose case in Pailha & Pouliquen (2009) is higher than the critical state solid volume fraction at equilibrium and thus could have been considered as dense. We still however keep calling this case loose in the following for consistency with Pailha &

Pouliquen (2009) and Bouchut et al. (2016). Note that the granular compaction represented by div v is one order of magnitude higher for low viscosity ($\sim 10^{-3}$) than for high viscosity ($\sim 10^{-4}$) (figure S11e,f).

S.D.3. *Test 1: Influence of the parameters on long-term stationary states*

In figure S8 the stationary states for the height of the mixture, velocity and concentration are presented as a function of three parameters around their reference values $a_\mu = 11.29$, $b_\varphi = 0.66$ and $I_0 = 0.279$ (Tapia et al. 2019). Only one parameter is varied while the others stay constant.

From the first row of figure S8, we can observe that the bigger influence of a_μ is on the velocity. On the other hand, the stationary velocities are independent of b_φ which has a bigger influence on the concentration. The third row shows that I_0 has only a small influence on all the quantities. Finally, we can also observe on the third column that all parameters have a small influence on the stationary height of the mixture.

In this figure the stationary solution for the case of the rheology considered in Bouchut et al. (2016) is also presented. We can observe that for bigger values of b_φ the stationary concentrations in the present model and in Bouchut et al. (2016) are close. In figure S9 the stationary solutions are represented as a function of a_μ, but with $b_\varphi/0.66 = 1.5$. In particular for $a_\mu/11.29 \approx 0.5$ the stationary solutions for the velocity, concentration and height of the mixture with the new rheology are very close to the solutions in Bouchut et al. (2016). Then, for the following tests in this paper we set $a_\mu = 11.29/2$, $b_\varphi = 0.66 \cdot 1.5$, $I_0 = 0.279$.

Figure S10 shows the evolution of the two dimensionless numbers in the rheology I^2 and J corresponding to test 5.1. For high and low viscosity cases J is bigger than I^2 and for the case of high viscosity I^2 is negligible.

S.D.4. *Test 3: Influence of the drag coefficient m_f in models of group A*

In the models of group A, there is a drag force between the mixture layer and the upper fluid layer. Taking a smaller drag $m_f = 0.1$ instead of $m_f = 1$ in equation (2.19) has almost no impact on the basal pressure or on the friction coefficient. It however significantly changes the velocities in the models as illustrated for $d = 10^{-2}$ m in figure S12c,d. Indeed, as the friction between the layers is smaller, the upper fluid moves faster and the mixture below moves slower. In this case, for $m_f = 0.1$, the granular phase stops after 2 s while it continues to move for $m_f = 1$ since it is entrained by the upper fluid. Similar behavior is observed for $d = 10^{-3}$ m. Interestingly, for $d = 10^{-2}$ m, the averaged velocity v_m in the two-layer models of group A with $m_f = 0.1$ is much closer to the one-layer models (group C) up to about 4 s. Afterwards v_m increases again for two-layer models as opposed to one-layer models (figure S12a,b).

Whatever the drag friction coefficient m_f, the forces are very similar in models (A1) and (A2) (figure S12e,f). At the beginning, the drag force between the layers is greater for $m_f = 1$ than for $m_f = 0.1$ but rapidly these forces reach about the same magnitude since even if $m_f = 0.1$ is smaller, the difference between the upper fluid and the mixture velocities is higher, leading to similar drag forces. As a result, even if the forces acting on the mixture layer are similar, the velocity distribution between the mixture and upper fluid layer is different for different m_f values. Figure S12e,f also clearly shows that the force related to the fluid exchange between the layers is small, but not negligible at the beginning of the flow.

S.D.5. *Test 3: Forces in models in uniform regime*

We present in the next table the forces applying to each model in the uniform regime, for equations written in conservative form. They are: solid bottom friction f_{fricsb}, fluid

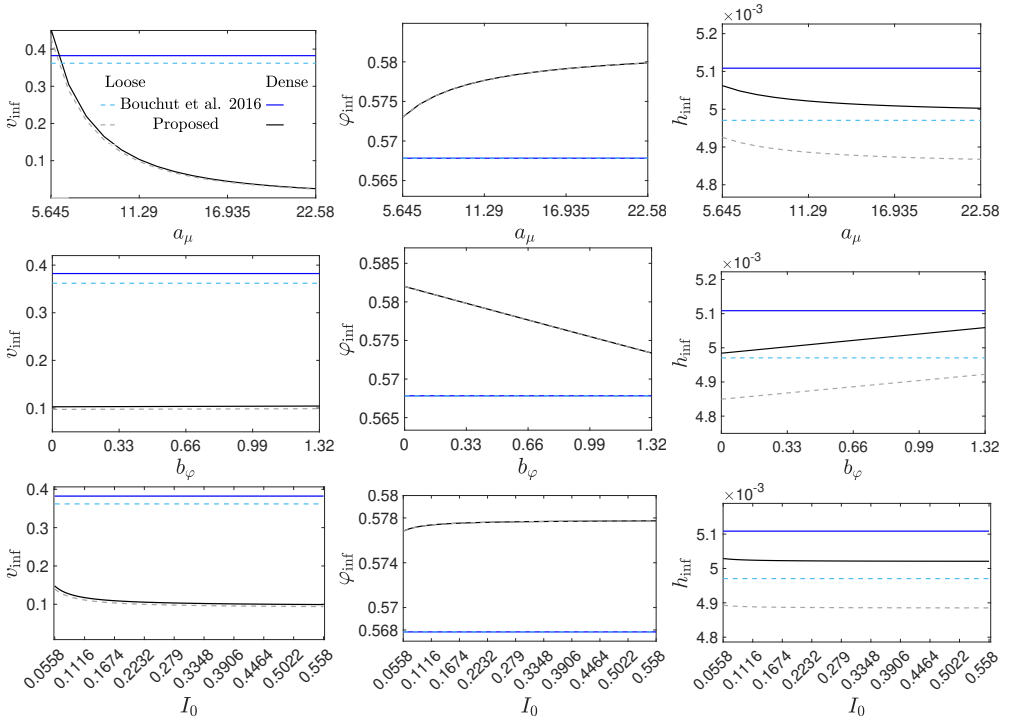

Figure S8: Long-term stationary states as a function of a_μ, b_φ, I_0: (first column) solid velocity $v_{\inf}$, (second column) concentration $\varphi_{\inf}$ and (third column) height of the mixture $h_{\inf}$ in the immersed simulations in section 5.1.

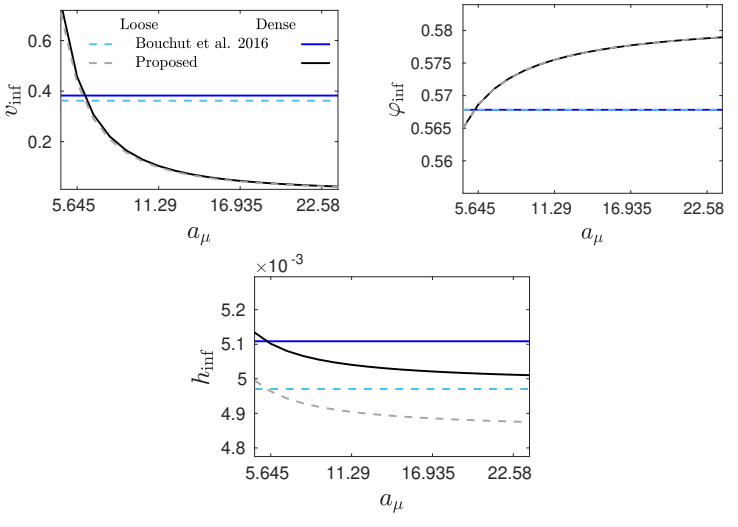

Figure S9: Long-term stationary states as a function of a_μ, b_φ, I_0, but now around reference values $I_0 = 0.279$ and $b_\varphi = 0.66 \times 1.5$: (first column) solid velocity $v_{\inf}$, (second column) concentration $\varphi_{\inf}$ and (third column) height of the mixture $h_{\inf}$ in the immersed simulations in section 5.1.

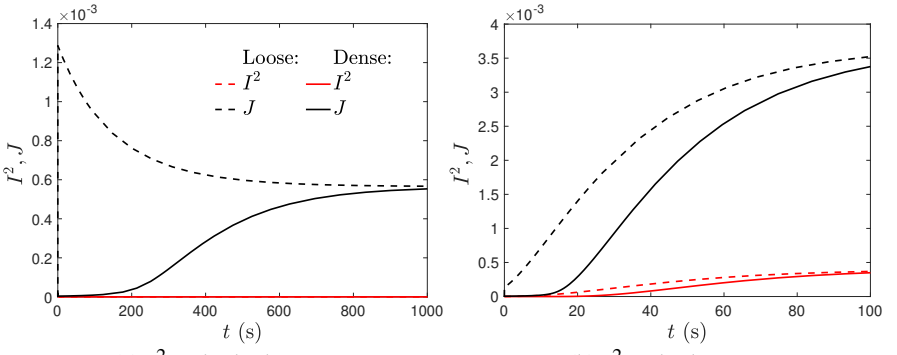

(a) I^2 and J high viscosity (b) I^2 and J low viscosity

Figure S10: Time change of I^2 and J for high and low viscosity cases in the immersed simulations in section 5.1.

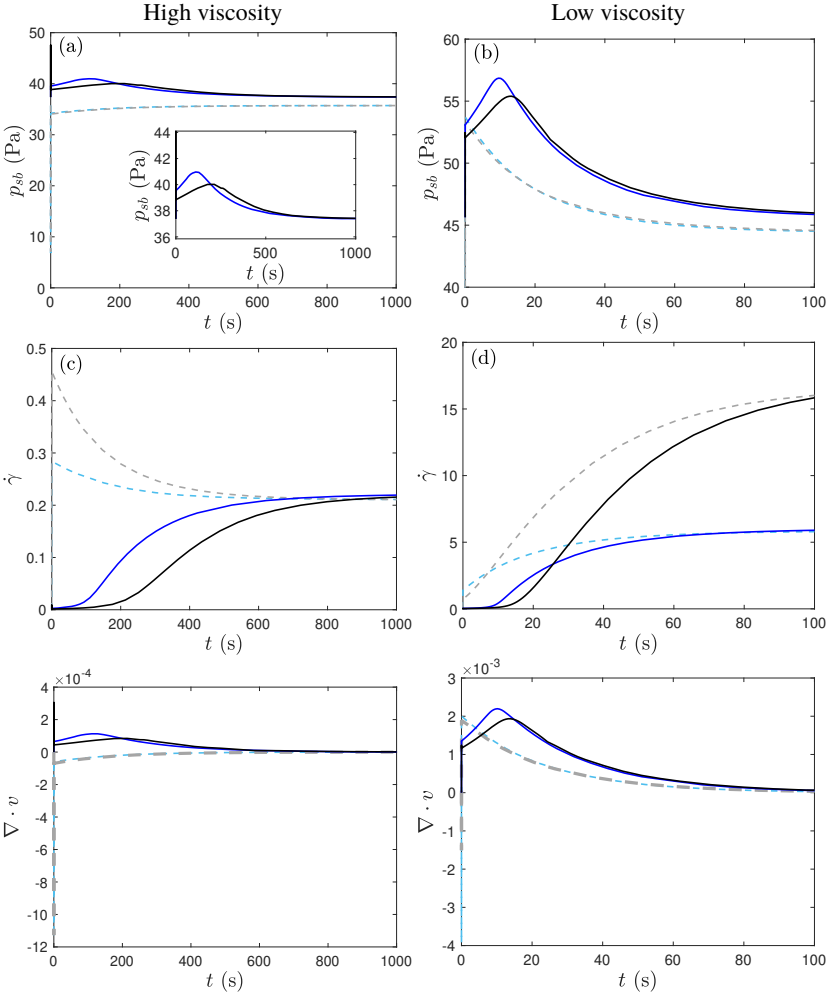

Figure S11: p_{sb} and $\dot{\gamma}$ in the high viscosity (left) and low viscosity case (right) in the immersed simulations in section 5.1, see figure 5.

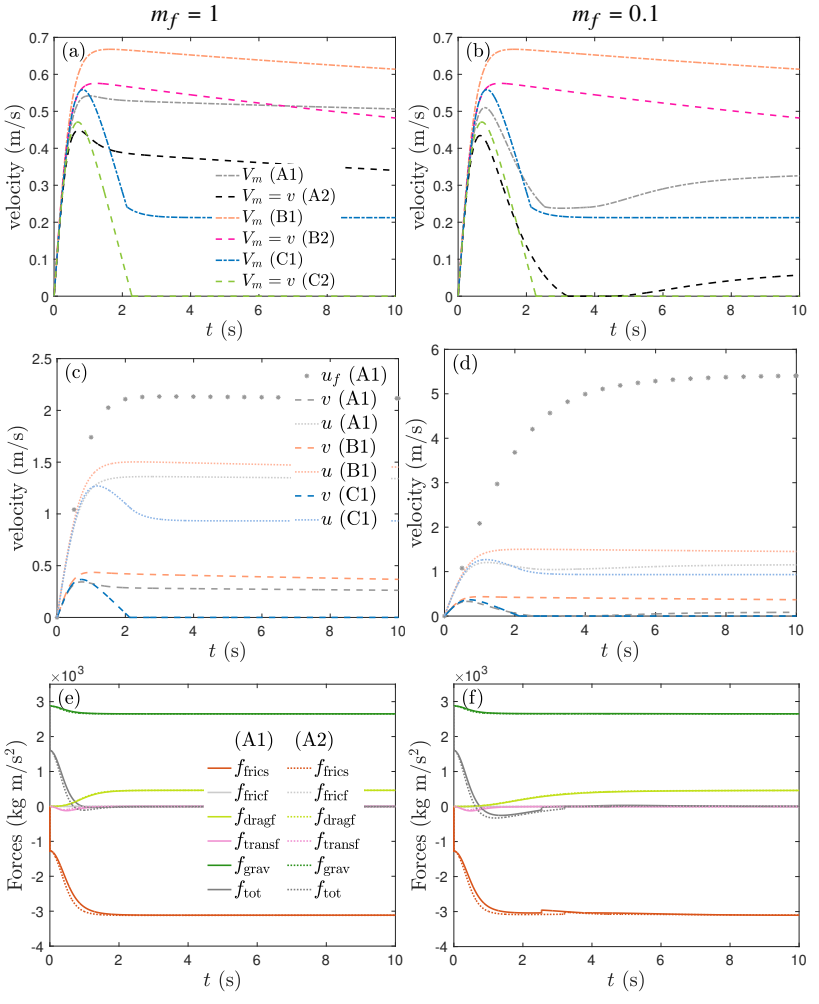

Figure S12: Loose case with slope angle $\theta = 13°$ for $C_h = 0.15$ and $d = 10^{-2}$ m. Comparison between all the models: those accounting for two velocities u, v in the mixture ((A1), (B1), and (C1)) and those assuming $u = v$ ((A2), (B2), and (C2)), for two drag coefficients: $m_f = 1$ (left column) and $m_f = 0.1$ (right column). (a)-(b) mixture velocity, (c)-(d) all velocities, (e)-(f) forces.

bottom friction f_{fricfb}, drag in the mixture f_{dragmix}, drag with fluid upper layer f_{dragf}, fluid transfer f_{transf}, gravity f_{grav}. Note that $k_f = \frac{\rho h_m \rho_f h_f}{\rho h_m + \rho_f h_f} |u_f - v_m|$ for the (A1) model and $k_f = \frac{\rho h_m \rho_f h_f}{\rho h_m + \rho_f h_f} |u_f - v|$ for the (A2) model. We denote f_{tot} the sum of all forces which represents the mass acceleration for each model which is equal to $\partial_t u$ in our uniform configuration.

Model		f_{fricsb}	f_{fricfb}	f_{dragmix}	f_{dragf}	f_{transf}	f_{grav}
(A1)	v	$-\mu\,\text{sgn}(v)p_{s_b}$	–	$\beta(u-v)h_m$	$k_f\frac{\rho_s\varphi}{\rho}(u_f-v_m)$	–	$-\rho_s\varphi h_m g\sin\theta$
	u	–	$-\frac{5}{2}\frac{\eta_e(1-\varphi)}{h_m}u$	$-\beta(u-v)h_m$	$k_f\frac{\rho_f(1-\varphi)}{\rho}(u_f-v_m)$	$((1-\lambda_f)u+\lambda_f u_f)\rho_f h_m\Phi$	$-\rho_f(1-\varphi)h_m g\sin\theta$
	u_f	–	–	–	$-k_f(u_f-v_m)$	$-((1-\lambda_f)u+\lambda_f u_f)\rho_f h_m\Phi$	$-\rho_f h_f g\sin\theta$
(B1)	v	$-\mu\,\text{sgn}(v)p_{s_b}$	–	$\beta(u-v)h_m$	–	–	$-\rho_s\varphi h_m g\sin\theta$
	u	–	$-\frac{5}{2}\frac{\eta_e(1-\varphi)}{h_m}u$	$-\beta(u-v)h_m$	–	$((1-\lambda_f)u+\lambda_f v_m)\rho_f h_m\Phi$	$-\rho_f(1-\varphi)h_m g\sin\theta$
	v_m	–	–	–	–	$-((1-\lambda_f)u+\lambda_f v_m)\rho_f h_m\Phi$	$-\rho_f h_f g\sin\theta$
(C1)	v	$-\mu\,\text{sgn}(v)p^*_{s_b}$	–	$\beta(u-v)H$	–	$-\frac{\rho_s\varphi}{\rho}((1-\lambda^*_f)u+\lambda^*_f v_m)\rho_f H\Phi$	$-\rho_s\varphi H g\sin\theta$
	u	–	$-\frac{5}{2}\frac{\eta_e(1-\varphi)}{H}u$	$-\beta(u-v)H$	–	$\frac{\rho_s\varphi}{\rho}((1-\lambda^*_f)u+\lambda^*_f v_m)\rho_f H\Phi$	$-\rho_f(1-\varphi)H g\sin\theta$
(A2)	v	$-\mu\,\text{sgn}(v)p_{s_b}$	$-\frac{5}{2}\frac{\eta_e(1-\varphi)}{h_m}v$	–	$k_f(u_f-v)$	$((1-\lambda_f)v+\lambda_f u_f)\rho_f h_m\Phi$	$-\rho h_m g\sin\theta$
	u_f	–	–	–	$-k_f(u_f-v)$	$((1-\lambda_f)v+\lambda_f u_f)\rho_f h_m\Phi$	$-\rho_f h_f g\sin\theta$
(B2)		$-\mu\,\text{sgn}(v)p_{s_b}$	$-\frac{5}{2}\frac{\eta_e(1-\varphi)}{h_m}v$	–	–	–	$-(\rho h_m+\rho_f h_f)g\sin\theta$
(C2)		$-\mu\,\text{sgn}(v)p^*_{s_b}$	$-\frac{5}{2}\frac{\eta_e(1-\varphi)}{H}v$	–	–	–	$-\rho H g\sin\theta$

Table S1: Forces for the uniform configuration for all models written from the conservative equations. They are: solid bottom friction f_{fricsb}, fluid bottom friction f_{fricfb}, drag in the mixture f_{dragmix}, drag with fluid upper layer f_{dragf}, fluid transfer f_{transf}, gravity f_{grav}. Note that $k_f = \frac{\rho h_m\rho_f h_f}{\rho h_m+\rho_f h_f}|u_f - v_m|$ for the (A1) model and $k_f = \frac{\rho h_m\rho_f h_f}{\rho h_m+\rho_f h_f}|u_f - v|$ for the (A2) model.

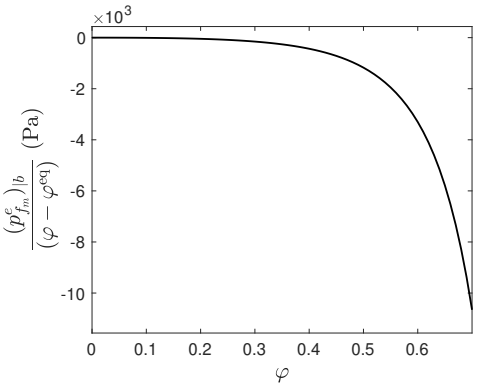

Figure S13: Illustration of the values of $(p^e_{f_m})_{|b}/(\varphi - \varphi^{\mathrm{eq}})$ defined in (2.36) as a function of φ for the parameters $\eta_f = 9.8 \times 10^{-3}$ Pa s, $d = 160$ μm, $K = 4.09$, $h_m = 5$ mm, $v = 0.4$ mm/s taken from Bouchut et al. (2016). Note that in Bouchut et al. (2016), $\varphi - \varphi^{\mathrm{eq}} \simeq 10^{-2}$.

S.E. Additional figures and tables

S.E.1. *Figures*

Figure S13 shows the values of $(p^e_{f_m})_{|b}/(\varphi - \varphi^{\mathrm{eq}})$ defined in (2.36) as a function of φ.
Figure S14 shows the comparison of the hydraulic permeability as a function of φ for the proposed model and for the Iverson-George model.

S.E.2. *Table: Equivalence of notations in our model and in Iverson & George (2014); George & Iverson (2014) and Meng & Wang (2018)*

In order to easily track the models' comparison we briefly summarize the equivalence between our notation and those used in the Iverson-George model (table S2), and in the Meng-Wang model (table S3), respectively. Note that we only display the variables that have a different notations in the models.

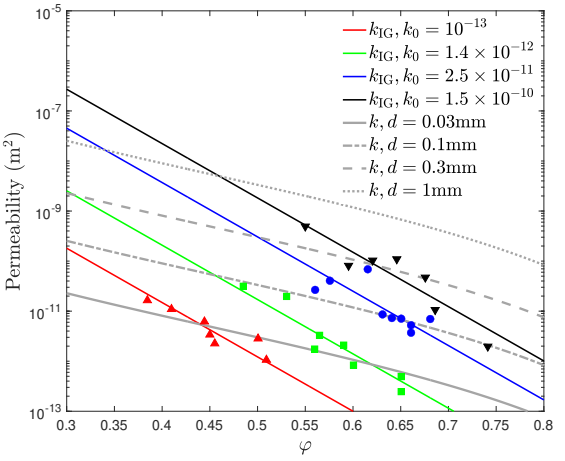

Figure S14: Comparison of the hydraulic permeability as a function of φ for the proposed model and for the Iverson-George model, given respectively by $k = \frac{(1-\varphi)^3 d^2}{150\varphi^2}$ m^2 in (2.21) and $k_{\mathrm{IG}} = k_0 e^{\frac{0.6-\varphi}{0.04}}$ m^2 in (3.18c), in a logarithmic scale for the y-axis. Values are taken from figure 5 in Iverson & George (2014) for different debris flows: red and green data correspond to real debris flows MSH and OSC where $d < 16$ mm, and $k_0 = 1.4 \times 10^{-12}$ m^2, $k_0 = 10^{-13}$ m^2 respectively, and blue and black data correspond to experiments SG and SGM where $d \sim 0.4 - 20$ mm, $k_0 = 1.5 \times 10^{-10}$ m^2 for SG, and $k_0 = 2.5 \times 10^{-11}$ m^2 (measured) and $k_0 = 5 \times 10^{-9}$ m^2 (for simulation in George & Iverson (2014)) for SGM.

Variable	**Here**	**Iverson-George**
Solid volume fraction	φ	m
Depth-averaged velocity	$\mathbf{v}$	(u, v)
Basal fluid pressure	$(p_{f_m})_{\|b}$	p_b
Excess pore fluid pressure	$p^e_{f_m}$	p_e
Effective fluid viscosity	η_e	μ
Internal friction angle	δ	ϕ
Dilatancy angle	ψ_{IG}	ψ
Static volume fraction	φ_c	m_{crit}
Critical-state compacity	$\varphi^{\mathrm{eq}}_{\mathrm{IG}}$	m_{eq}
Viscous dimensionless number	J	I_{v}
Stokes number	St	S

Table S2: Equivalence between our notations and those used in the Iverson-George model (Iverson & George 2014; George & Iverson 2014). Note that in George & Iverson (2014) the "bar" notation is removed in the depth-averaged velocity.

Variable	**Here**	**Meng & Wang**
Solid density	$\varphi\rho_s$	ρ_s
Fluid density	$(1-\varphi)\rho_f$	ρ_f
Material density ($j = s, f$)	ρ_j	$\tilde{\rho}_j$
Dynamic fluid viscosity	η_f	μ_f
Solid volume fraction	φ	ν_s
Fluid volume fraction	$1-\varphi$	ν_f
Solid velocity (3-D)	$\mathbf{V} = (\mathbf{v}^{\mathbf{x}}, v^z)$	$\mathbf{v}_s = (u_s, v_s, w_s)$
Fluid velocity (3-D)	$\mathbf{U} = (\mathbf{u}^{\mathbf{x}}, u^z)$	$\mathbf{v}_f = (u_f, v_f, w_f)$
Solid velocity (averaged)	$\mathbf{v}$	u_s
Fluid velocity (averaged)	$\mathbf{u}$	u_f
Mixture velocity (averaged)	$\mathbf{v}_m$	$\mathbf{v}_m$
Solid stress tensor	$\varphi\sigma_s$	$\boldsymbol{\sigma}_e$
Fluid stress tensor	$(1-\varphi)\sigma_{f_m}$	$\boldsymbol{\sigma}_f$
Shear fluid stress tensor	σ'_{f_m}	$\boldsymbol{\tau}_f$
Excess pore fluid pressure (averaged)	$p^e_{f_m}$	p_e
Solid pressure (averaged)	p_s	$\sigma_0 = \sigma_{e(zz)}$
Mass exchange term (flux of the granular mass)	$\Im$	$\mathcal{J}$
Mass exchange distribution coeff.	λ_f	λ
Solid friction coef.	–	α_s
Fluid friction coef.	$\frac{5}{2}\frac{\eta_e}{h_m}$	α_f
Coulomb friction coef.	μ	μ_s

Table S3: Equivalence between our notations and those used in the Meng-Wang model (Meng & Wang 2018)

REFERENCES

Allstadt, K., Matoza, R., Lockhart, A., Moran, S., Caplan-Auerbach, J. & Haney, M. 2018 Seismic and acoustic signatures of surficial mass movements at volcanoes. *J. Volcanol. Geotherm. Res.* **364**.

Amarsid, L., Delenne, J.-Y., Mutabaruka, P., Monerie, Y., Perales, F. & Radjai, F. 2017 Viscoinertial regime of immersed granular flows. *Physical Review E* **96** (1), 012901.

Athani, S., Metzger, B., Forterre, Y. & Mari, R. 2022 Transient flows and migration in granular suspensions: key role of reynolds-like dilatancy. *Journal of Fluid Mechanics* **949**, A9.

Barker, T., Gray, J.M.N.T., Schaeffer, D.G. & Shearer, M. 2023 Well-posedness and ill-posedness of single-phase models for suspensions. *Journal of Fluid Mechanics* **954**, A17.

Barker, T., Schaeffer, D. G., Bohorquez, P. & Gray, J. M. N. T. 2015 Well-posed and ill-posed behaviour of the μ(I)-rheology for granular flow. *Journal of Fluid Mechanics* **779**, 794–818.

Baumgarten, Aaron S. & Kamrin, Ken 2019 A general fluid–sediment mixture model and constitutive theory validated in many flow regimes. *Journal of Fluid Mechanics* **861**, 721–764.

Benzoni-Gavage, Sylvie & Serre, Denis 2006 Multi-dimensional hyperbolic partial differential equations: First-order systems and applications. Oxford University Press.

de Boer, R. & Ehlers, W. 1990 The development of the concept of effective stresses. *Acta Mechanica* **83** (1), 77–92.

Bouchut, F., Fernández-Nieto, E. D., Mangeney, A. & Lagrée, P. Y. 2008 On new erosion models of savage–hutter type for avalanches. *Acta Mechanica* **199** (1), 181–208.

Bouchut, F., Fernández-Nieto, E. D., Mangeney, A. & Narbona-Reina, G. 2015 A two-phase shallow debris flow model with energy balance. *ESAIM: M2AN* **49** (1), 101–140.

Bouchut, F., Fernández-Nieto, E. D., Mangeney, A. & Narbona-Reina, G. 2016 A two-phase two-layer model for fluidized granular flows with dilatancy effects. *Journal of Fluid Mechanics* **801**, 166–221.

Bouchut, F., Fernández-Nieto, E.D., Koné, E.H., Mangeney, A. & Narbona-Reina, G. 2021 Dilatancy in dry granular flows with a compressible $\mu(i)$ rheology. *Journal of Computational Physics* **429**, 110013.

Boyer, F., Guazzelli, E. & Pouliquen, O. 2011 Unifying suspension and granular rheology. *Physical Review Letters* **107** (18), 188301.

Cassar, C., Nicolas, M. & Pouliquen, O. 2005 Submarine granular flows down inclined planes. *Physics of Fluids* **17** (10), 103301.

Chauchat, J. & Médale, M. 2010 A three-dimensional numerical model for incompressible two-phase flow of a granular bed submitted to a laminar shearing flow. *Computer Methods in Applied Mechanics and Engineering* **199** (9–12), 439–449.

Dafalias, Yannis F. & Manzari, Majid T. 2004 Simple plasticity sand model accounting for fabric change effects. *Journal of Engineering Mechanics* **130** (6), 622–634.

Drach, Elias 2023 Shallow-water type models for wet debris flows with dilatancy. PhD thesis, Université Gustave-Eiffel (Paris).

Einstein, A. 1906 A new determination of molecular dimensions. *Ann.d.Phys* **19**, 289–306.

Engelund, F. 1953 On the laminar and turbulent flows of ground water through homogeneous sand. Danish Academy of Technical Sciences / Transactions 3. Akademiet for de tekniske videnskaber.

Garres-Díaz, J., Bouchut, F., Fernández-Nieto, E.D., Mangeney, A. & Narbona-Reina, G. 2020 Multilayer models for shallow two-phase debris flows with dilatancy effects. *Journal of Computational Physics* **419**, 109699.

George, D.L. & Iverson, R.M. 2014 A depth-averaged debris-flow model that includes the effects of evolving dilatancy. II. Numerical predictions and experimental tests. *Proceedings of the Royal Society A: Mathematical, Physical and Engineering Sciences* **470** (2170), 20130820, arXiv: https://royalsocietypublishing.org/doi/pdf/10.1098/rspa.2013.0820.

Holtzman, R., Silin, D. B. & Patzek, T. W. 2009 Mechanical properties of granular materials: A variational approach to grain-scale simulations. *International Journal for Numerical and Analytical Methods in Geomechanics* **33** (3), 391–404, arXiv: https://onlinelibrary.wiley.com/doi/pdf/10.1002/nag.725.

Hungr, Oldrich & McDougall, Scott 2009 Two numerical models for landslide dynamic analysis. *Computers & Geosciences* **35** (5), 978–992.

Iverson, Richard M. 1997 The physics of debris flows. *Reviews of Geophysics* **35** (3), 245–296.

Iverson, R. M. & George, D. L. 2014 A depth-averaged debris-flow model that includes the effects of evolving dilatancy. I. Physical basis. *Proceedings of the Royal Society A: Mathematical, Physical and Engineering Sciences* **470** (2170), 20130819, arXiv: https://royalsocietypublishing.org/doi/pdf/10.1098/rspa.2013.0819.

Iverson, Richard M., Logan, Matthew, LaHusen, Richard G. & Berti, Matteo 2010 The perfect debris flow? aggregated results from 28 large-scale experiments. *Journal of Geophysical Research: Earth Surface* **115** (F3), arXiv: https://agupubs.onlinelibrary.wiley.com/doi/pdf/10.1029/2009JF001514.

Iverson, R. M., Reid, M. E., Iverson, N. R., LaHusen, R. G., Logan, M., Mann, J. E. & Brien, D. L. 2000 Acute sensitivity of landslide rates to initial soil porosity. *Science* **290** (5491), 513–516, arXiv: https://www.science.org/doi/pdf/10.1126/science.290.5491.513.

Jackson, R. 2000 The Dynamics of Fluidized Particles. Cambridges Monographs on Mechanics. Cambridge University Press.

Lee, Cheng-Hsien 2021 Two-phase modelling of submarine granular flows with shear-induced volume change and pore-pressure feedback. *Journal of Fluid Mechanics* **907**, A31.

Leonardi, Alessandro, Cabrera, Miguel, Wittel, Falk K., Kaitna, Roland, Mendoza, Miller, Wu, Wei & Herrmann, Hans J. 2015 Granular-front formation in free-surface flow of concentrated suspensions. *Phys. Rev. E* **92**, 052204.

Luca, I., Kuo, C. Y., Hutter, K. & Tai, Y. C. 2012 Modeling Shallow Over-Saturated Mixtures on Arbitrary Rigid Topography. *Journal of Mechanics* **28** (3), 523–541, arXiv: https://academic.oup.com/jom/article-pdf/28/3/523/34414019/jom_v28_3_523.pdf.

Lucas, A., Mangeney, A. & Ampuero, J. P. 2014 Frictional velocity-weakening in landslides on earth and on other planetary bodies. *Nature Communications* **5** (3417).

M. Pelanti, F. Bouchut & A. Mangeney 2008 A Roe-type scheme for two-phase shallow granular flows over variable topography. *ESAIM: M2AN* **42** (5), 851–885.

Mangeney, A., Bouchut, F., Thomas, N., Vilotte, J. P. & Bristeau, M. O. 2007 Numerical modeling of self-channeling granular flows and of their levee-channel deposits. *Journal of Geophysical Research: Earth Surface* **112** (F2), n/a–n/a, f02017.

Mangeney-Castelnau, A., Vilotte, J.-P., Bristeau, M. O., Perthame, B., Bouchut, F., Simeoni, C. & Yerneni, S. 2003 Numerical modeling of avalanches based on Saint Venant equations using a kinetic scheme. *Journal of Geophysical Research: Solid Earth* **108** (B11), n/a–n/a, 2527.

Meng, Xiannan, Johnson, C.G. & Gray, J.M.N.T. 2022 Formation of dry granular fronts and watery tails in debris flows. *Journal of Fluid Mechanics* **943**, A19.

Meng, X., Taylor-Noonan, A.M., Johnson, C.G., Take, W.A., Bowman, E.T. & Gray, J.M.N.T. 2024 Granular-fluid avalanches: the role of vertical structure and velocity shear. *Journal of Fluid Mechanics* **980**, A11.

Meng, X. & Wang, Y. 2018 Modeling dynamic flows of grain–fluid mixtures by coupling the mixture theory with a dilatancy law. *Acta Mech* **229** (6), 2521–2538.

Meng, X., Wang, Y., Wang, C. & Fisher, J-T. 2017 Modeling of unsaturated granular flows by a two-layer approach. *Acta Geotechnica* **12** (3), 677–701.

Montellà, E.P., Chauchat, J., Bonamy, C., Weij, D., Keetels, G.H. & Hsu, T.J. 2023 Numerical investigation of mode failures in submerged granular columns. *Flow* **3**, E28.

Montellà, E.P., Chauchat, J., Chareyre, B., Bonamy, C. & Hsu, T.J. 2021 A two-fluid model for immersed granular avalanches with dilatancy effects. *Journal of Fluid Mechanics* **925**, A13.

Moretti, L., Allstadt, K., Mangeney, A., Capdeville, Y., Stutzmann, E. & Bouchut, F. 2015 Numerical modeling of the mount meager landslide constrained by its force history derived from seismic data. *Journal of Geophysical Research: Solid Earth* **120** (4), 2579–2599, arXiv: https://agupubs.onlinelibrary.wiley.com/doi/pdf/10.1002/2014JB011426.

Moretti, L., Mangeney, A., Capdeville, Y., Stutzmann, E., Huggel, C., Schneider, D. & Bouchut, F. 2012 Numerical modeling of the mount steller landslide flow history and of the generated long period seismic waves. *Geophysical Research Letters* **39** (16), arXiv: https://agupubs.onlinelibrary.wiley.com/doi/pdf/10.1029/2012GL052511.

Ouriemi, Malika, Aussillous, Pascale & Guazzelli, Elisabeth 2009 Sediment dynamics. part 1. bed-load transport by laminar shearing flows. *Journal of Fluid Mechanics* **636**, 295–319.

Pailha, M., Nicolas, M. & Pouliquen, O. 2008 Initiation of underwater granular avalanches: Influence of the initial volume fraction. *Physics of Fluids* **20** (11), 111701.

Pailha, M. & Pouliquen, O. 2009 A two-phase flow description of the initiation of underwater granular avalanches. *Journal of Fluid Mechanics* **633**, 115–135.

Patra, Abani, Bevilacqua, Andrea, Akhavan-Safaei, Ali, Pitman, E. Bruce, Bursik, Marcus & Hyman, David 2020 Comparative analysis of the structures and outcomes of geophysical flow models and modeling assumptions using uncertainty quantification. *Frontiers in Earth Science* **8**.

Pelanti, Marica, Bouchut, François & Mangeney, Anne 2011 A riemann solver for single-phase and

two-phase shallow flow models based on relaxation. relations with roe and vfroe solvers. *Journal of Computational Physics* **230** (3), 515–550.

Peruzzetto, M., Komorowski, J.C., Le Friant, A., Rosas-Carbajal, M., Mangeney, A. & Legendre, Y. 2019 Modeling of partial dome collapse of la soufrière of guadeloupe volcano: implications for hazard assessment and monitoring. *Scientific Reports* **9** (1), 13105.

Peruzzetto, M., Levy, C., Thiery, Y., Grandjean, G., Mangeney, A., Lejeune, A.M., Nachbaur, A., Legendre, Y., Vittecoq, B., Saurel, J.M., Clouard, V., Dewez, T., Fontaine, F.R., Mergili, M., Lagarde, S., Komorowski, J.C., Le Friant, A. & Lemarchand, A. 2022 Simplified simulation of rock avalanches and subsequent debris flows with a single thin-layer model: Application to the prêcheur river (martinique, lesser antilles). *Engineering Geology* **296**, 106457.

Peruzzetto, M., Mangeney, A., Bouchut, F., Grandjean, G., Levy, C., Thiery, Y. & Lucas, A. 2021 Topography curvature effects in thin-layer models for gravity-driven flows without bed erosion. *Journal of Geophysical Research: Earth Surface* **126** (4), e2020JF005657, e2020JF005657 2020JF005657, arXiv: https://agupubs.onlinelibrary.wiley.com/doi/pdf/10.1029/2020JF005657.

Pitman, E.B. & Le, L. 2005 A two-fluid model for avalanche and debris flows. *Philosophical Transactions of the Royal Society of London A: Mathematical, Physical and Engineering Sciences* **363** (1832), 1573–1601, arXiv: http://rsta.royalsocietypublishing.org/content/363/1832/1573.full.pdf.

Poulain, P, Friant, A Le, Mangeney, A, Viroulet, S, Fernandez-Nieto, E, Castro Diaz, M, Peruzzetto, M, Grandjean, G, Bouchut, F, Pedreros, R & Komorowski, J-C 2022 Performance and limits of a shallow-water model for landslide-generated tsunamis: from laboratory experiments to simulations of flank collapses at Montagne Pelée (Martinique). *Geophysical Journal International* **233** (2), 796–825, arXiv: https://academic.oup.com/gji/article-pdf/233/2/796/48496045/ggac482.pdf.

Pudasaini, S. P., Wang, Y. & Hutter, K. 2005 Modelling debris flows down general channels. *Natural Hazards and Earth System Sciences* **5** (6), 799–819.

Rondon, L., Pouliquen, O. & Aussillous, P. 2011 Granular collapse in a fluid: Role of the initial volume fraction. *Physics of Fluids* **23** (7), 073301, arXiv: https://pubs.aip.org/aip/pof/article-pdf/doi/10.1063/1.3594200/15798232/073301_1_online.pdf.

Roux, S. & Radjai, F. 1998 Texture-Dependent Rigid-Plastic Behavior, pp. 229–236. Dordrecht: Springer Netherlands.

Savage, S. B. & Hutter, K. 1989 The motion of a finite mass of granular material down a rough incline. *Journal of Fluid Mechanics* **199**, 177–215.

Schaeffer, D. G., Barker, T., Tsuji, D., Gremaud, P., Shearer, M. & Gray, J. M. N. T. 2019 Constitutive relations for compressible granular flow in the inertial regime. *Journal of Fluid Mechanics* **874**, 926–951.

Sun, W., Meng, X., Wang, Y., Hsiau, S. S. & You, Z. 2023 A depth-averaged description of submarine avalanche flows and induced surface waves. *Journal of Geophysical Research: Earth Surface* **128** (4), e2022JF006893, e2022JF006893 2022JF006893, arXiv: https://agupubs.onlinelibrary.wiley.com/doi/pdf/10.1029/2022JF006893.

Tapia, Franco, Ichihara, Mie, Pouliquen, Olivier & Guazzelli, Élisabeth 2022 Viscous to inertial transition in dense granular suspension. *Phys. Rev. Lett.* **129**, 078001.

Tapia, Franco, Pouliquen, Olivier & Guazzelli, Élisabeth 2019 Influence of surface roughness on the rheology of immersed and dry frictional spheres. *Phys. Rev. Fluids* **4**, 104302.

Trulsson, Martin, Andreotti, Bruno & Claudin, Philippe 2012 Transition from the viscous to inertial regime in dense suspensions. *Physical Review Letters* **109** (11), 118305.